ARMY RESEARCH LABORATORY

Standoff Variation Study I: Detonation of a Donor Munitions Stack and Responses of a Trapezoidal Water Barricade and an Acceptor Stack

Richard E. Lottero

ARL-TR-1943 May 1999

The findings in this report are not to be construed as an official Department of the Army position unless so designated by other authorized documents.

Citation of manufacturer's or trade names does not constitute an official endorsement or approval of the use thereof.

Destroy this report when it is no longer needed. Do not return it to the originator.

Army Research Laboratory
Aberdeen Proving Ground, MD 21005-5066

ARL-TR-1943 **May 1999**

Standoff Variation Study I: Detonation of a Donor Munitions Stack and Responses of a Trapezoidal Water Barricade and an Acceptor Stack

Richard E. Lottero
Weapons and Materials Research Directorate, ARL

Abstract

This report documents the fully coupled numerical modeling of the detonation of a simplified munitions stack in a temporary storage area and the subsequent effects on the immediate surroundings of the stack. Five plausible configurations of this munitions stack, referred to as the "donor" stack, an intervening water barricade, and an "acceptor" munitions stack are modeled in two-dimensional (2-D) Cartesian hydrocode computations using the CTH hydrodynamics computer code. The distance between each munitions stack and the barricade, referred to here as the "standoff" distance, is varied from one computation to the next, with the physical characteristics of the munitions stacks and barricade themselves remaining unchanged. The donor stack is modeled as an uncased, condensed, high-explosive charge with a rectangular cross section. The water barricade has a trapezoidal cross section, and the acceptor stack is a solid iron rectangle. The loadings on both the barricade and the acceptor stack are computed, as are their fully coupled responses to those loadings. Only a relatively weak inverse functional relationship with standoff distance was found in the barricade response. A moderate correlation with standoff distance, and a stronger correlation with the distance between the donor stack right face and the acceptor stack left face, were found for the acceptor stack response. The results are also compared with those of an earlier study on two uncoupled blast loading and response computations for one of the configurations.

ACKNOWLEDGMENTS

Technical consultation on the selection of munitions to be modeled and on munitions storage layouts was provided by Drs. Robert Frey and John Starkenberg of the U.S. Army Research Laboratory (ARL). Technical consultation and support in the use of the latest versions of the CTH hydrodynamics computer code were provided by Messrs. Stephen Schraml and Kent Kimsey of ARL and Dr. Eugene Hertel of Sandia National Laboratories (SNL). Technical and financial support were provided by Mr. Duane Scarborough of the U.S. Army Defense Ammunition Logistics (Ammolog) Activity. Their assistance and support are gratefully acknowledged.

INTENTIONALLY LEFT BLANK

TABLE OF CONTENTS

		Page
	LIST OF FIGURES	vii
	LIST OF TABLES	xi
1.	INTRODUCTION	1
2.	COMPUTATIONAL APPROACH AND GEOMETRY	2
2.1.	General Comments on the Hydrocode Model	2
2.2.	The Donor Munitions Stack	3
2.3.	The Barricade	5
2.4.	The Acceptor Munitions Stack	5
3.	THE HYDROCODE COMPUTATIONS	6
3.1.	Flow Field Development	6
3.2.	Barricade Dynamics	24
3.3.	Acceptor Stack Dynamics	37
3.4.	Acceptor Stack Left Surface Pressures	44
3.5.	Coupled Versus Uncoupled Acceptor Stack Dynamics at 3.05-m Standoff	48
4.	CONCLUSION	54
	REFERENCES	57
	DISTRIBUTION LIST	59
	REPORT DOCUMENTATION PAGE	63

INTENTIONALLY LEFT BLANK

LIST OF FIGURES

Figure		Page
1	Flow Field at Time = 0.0 for Computation 980505, 3.05-m Standoff	7
2	Flow Field at Time = 2.5 ms for Computation 980505, 3.05-m Standoff . . .	8
3	Flow Field at Time = 5.0 ms for Computation 980505, 3.05-m Standoff . . .	10
4	Flow Field at Time = 7.5 ms for Computation 980505, 3.05-m Standoff . . .	11
5	Flow Field at Time = 10.0 ms for Computation 980505, 3.05-m Standoff . .	12
6	Flow Field at Time = 12.5 ms for Computation 980505, 3.05-m Standoff . .	13
7	Flow Field at Time = 15.0 ms for Computation 980505, 3.05-m Standoff . .	14
8	Flow Field at Time = 20.0 ms for Computation 980505, 3.05-m Standoff . .	16
9	Flow Field at Time = 30.0 ms for Computation 980505, 3.05-m Standoff . .	17
10	Flow Field at Time = 40.0 ms for Computation 980505, 3.05-m Standoff . .	18
11	Flow Field at Time = 0.0 for Computation 980521, 2.50-m Standoff	19
12	Flow Field at Time = 10.0 ms for Computation 980521, 2.50-m Standoff . .	20
13	Flow Field at Time = 20.0 ms for Computation 980521, 2.50-m Standoff . .	21
14	Flow Field at Time = 30.0 ms for Computation 980521, 2.50-m Standoff . .	22
15	Flow Field at Time = 40.0 ms for Computation 980521, 2.50-m Standoff . .	23
16	Flow Field at Time = 0.0 for Computation 980610, 2.00-m Standoff	25
17	Flow Field at Time = 10.0 ms for Computation 980610, 2.00-m Standoff . .	26
18	Flow Field at Time = 20.0 ms for Computation 980610, 2.00-m Standoff . .	27
19	Flow Field at Time = 30.0 ms for Computation 980610, 2.00-m Standoff . .	28
20	Flow Field at Time = 40.0 ms for Computation 980610, 2.00-m Standoff . .	29
21	Water Barricade X-Direction Momentum Toward Acceptor Stack for Computations 980505 Through 980610	30
22	Water Barricade X-Direction Velocity Toward the Acceptor Stack for Computations 980505 Through 980610	32
23	Water Barricade X-Direction Acceleration Toward the Acceptor Stack for Computations 980505 Through 980610	33

LIST OF FIGURES (continued)

Figure		Page
24	Water Barricade Initial X-Direction Acceleration Toward the Acceptor Stack for Computations 980505 Through 980610	33
25	Water Barricade Left Surface X-Direction Total Impulse per Meter Depth for Computations 980505 Through 980610	34
26	Water Barricade X-Direction Distance Moved Toward the Acceptor Stack for Computations 980505 Through 980610	35
27	Normalized (Direct Ratio) Barricade Parameters Versus Standoff Distance for Computations 980505 Through 980610	36
28	Normalized (Direct Ratio) Barricade Parameters Versus Normalized (Indirect Ratio) Standoff Distance for Computations 980505 Through 980610	36
29	Acceptor Stack X-Direction Momentum for Computations 980505 Through 980610	37
30	Acceptor Stack X-Direction Velocity, Computations 980505 Through 980610	39
31	Acceptor Stack X-Direction Acceleration for Computations 980505 Through 980610	39
32	Acceptor Stack X-Direction Total Impulse per Meter Depth for Computations 980505 Through 980610	40
33	Acceptor Stack X-Direction Distance Moved for Computations 980505 Through 980610	41
34	Normalized (Direct Ratio) Acceptor Stack Parameters Versus Standoff Distance for Computations 980505 Through 980610	42
35	Normalized (Direct Ratio) Acceptor Stack Parameters Versus Normalized (Inverse Ratio) Standoff Distance for Computations 980505 Through 980610	43
36	Normalized (Direct Ratio) Acceptor Stack Parameters Versus Face Separation for Computations 980505 Through 980610	44
37	Normalized (Direct Ratio) Acceptor Stack Parameters Versus Normalized (Inverse Ratio) Face Separation for Computations 980505 Through 980610	45
38	Acceptor Stack Left Surface Overpressure, 3.05-m Standoff, Computation 980505	45
39	Acceptor Stack Left Surface Overpressure, 2.75-m Standoff, Computation 980507	46

LIST OF FIGURES (continued)

Figure		Page
40	Acceptor Stack Left Surface Overpressure, 2.50-m Standoff, Computation 980521	47
41	Acceptor Stack Left Surface Overpressure, 2.25-m Standoff, Computation 980528	47
42	Acceptor Stack Left Surface Overpressure, 2.00-m Standoff, Computation 980610	48
43	Acceptor Stack X-Direction Momentum, Coupled Versus Uncoupled Computations, 3.05-m Standoff	49
44	Acceptor Stack X-Direction Velocity, Coupled Versus Uncoupled Computations, 3.05-m Standoff	50
45	Acceptor Stack X-Direction Acceleration, Coupled Versus Uncoupled Computations, 3.05-m Standoff	51
46	Acceptor Stack X-Direction Total Impulse per Meter Depth, Coupled Versus Uncoupled Computations, 3.05-m Standoff	52
47	Acceptor Stack X-Direction Distance Moved, Coupled Versus Uncoupled Computations, 3.05-m Standoff	52
48	Acceptor Stack Left Surface Overpressure, 3.05-m Standoff, Coupled Computation 980505 (Rescaled)	53
49	Acceptor Stack Left Surface Overpressure, 3.05-m Standoff, Uncoupled Computation 971001	54

INTENTIONALLY LEFT BLANK

LIST OF TABLES

Table		Page
1	Barricade Peak X-Direction Bulk Motion Parameters	31
2	Acceptor Stack Peak X-Direction Bulk Motion Parameters	38

INTENTIONALLY LEFT BLANK

1. INTRODUCTION

This report documents the extension of an earlier study, described in detail[1] and later summarized[2] in previous publications, of the detonation of a single munitions stack, the "donor" stack, within a postulated munitions temporary storage area and the subsequent effects on its surroundings. In that study, the remaining stacks, the "acceptor" stacks, were presumed to be separated from the donor stack and one another by water-filled barricades designed to be rapidly erected by fielded military units during rapid-deployment or rapid-movement operations. The separation distance between a munitions stack, either a donor or an acceptor, and a barricade is the "standoff," measured from the base of the munitions stack to the base of the barricade. The primary purpose of protective barricades is to prevent a direct, line-of-sight path from existing for either blast or fragments between munitions stacks in proximity to one another. Equally important, the impact of any part of a barricade on an acceptor stack must not cause an initiation in the acceptor stack. The barricade design is one of the designs currently being evaluated by the U.S. Army Research Laboratory (ARL) on behalf of its customer, the U.S. Army Defense Ammunition Logistics (Ammolog) Activity.

Military units operating in rapidly changing situations typically cannot store munitions using standard safe-distance guidelines normally applicable for permanent storage in a safe area. Munitions must be readily accessible for either use or relocation with minimal delay. At times such as these, it is sometimes considered necessary by commanders in the field to store munitions in closely spaced stacks in the open with no protective barricades between them. An incidence of extremely close spacing of munitions stacks with no barricading that occurred in the buildup of ammunition stocks at the port of Al Jubayl, Saudia Arabia, before the opening of hostilities in the Gulf War was cited in an earlier report.[1] Fortunately, no initiating incident occurred. The same earlier report included, as examples of what can occur, photographs showing some of the destruction at Doha, Kuwait, in 1991 after a fire started a chain reaction among unprotected, closely spaced munitions stacks.

The earlier report[1] presented the results of two uncoupled computations using the "June_96" version[3, 4] of the CTH[5] hydrocode. The first, designated as "Computation 970908," primarily focused on the munitions stack detonation and the loading and response of the barricade. The loading on the acceptor stack in that computation was almost exclusively from the air shock that diffracted over the barricade and was minimal. The second computation, "Computation 971001," modeled the barricade, reconstituted into its original shape and traveling at its late-time bulk velocity from the first computation, striking the acceptor stack. This computational decoupling was necessary because stability problems in the June_96 version would not allow a single, fully coupled computation to proceed from the time of the initiation of the donor stack to the completion of the impact of the loaded and subsequently distorted barricade on the acceptor stack. The first of these two computations produced a reasonably good estimate of the reaction of the barricade to the detonation of the mathematically simplified donor stack. However, the uncoupled nature of the second computation meant that the computed loading on and response of the acceptor stack included

(possible) unquantified errors beyond those that are normal and inevitable in any hydrocode simulation.

This report describes a series of computations for five different standoff distances. The donor stack, acceptor stack, and barricade are modeled in a way that is identical to that used in the previous study.[1] All computations are fully coupled in the sense that the detonation of the munitions stack; the blast loading on and response of the barricade; and loading from all sources on and the response of acceptor stack are modeled in a single, continuous computation. The first computation, "Computation 980505," connects these computations to those in the previous study because it models in a single computation that which was modeled in an uncoupled way by Computations 970908 and 971001. Thus, any error introduced by simulating that first configuration with a standoff distance of 3.048 m (10.0 ft) (hereinafter rounded to 3.05 m for simplicity, except when specifically used to calculate a parameter) with two uncoupled computations can be quantified. The next four computations were run with successively smaller standoff distances: 2.75 m for Computation 980507, 2.50 m for Computation 980521, 2.25 m for Computation 980528, and 2.00 m for Computation 980610.

2. COMPUTATIONAL APPROACH AND GEOMETRY

2.1. General Comments on the Hydrocode Model

The five coupled computations that are reported here were performed using the then-latest general-release version, CTH_9801, of the CTH[6, 7] hydrocode developed at Sandia National Laboratories (SNL). It also includes the May 1998 and August 1998 "patches" (i.e., coding updates) that were released by SNL. CTH solves the inviscid Euler equations using a second-order accurate, explicit time-stepping method. It has a Lagrangian first phase and a second phase that uses a mesh remapping to bring the distorted mesh back to the stationary Eulerian mesh and thereby perform a second-order accurate fluxing of materials between cells. The conservation equations are replaced by finite-volume approximations to maximize the code's ability to conserve mass, momentum, and energy. The computational grid cells have rectangular cross sections in two-dimensional (2-D) Cartesian coordinates with a presumed unit depth (1.0 cm). This unit depth represents an infinite depth with no wave interactions or fluxing in that direction. The computational grid cells in three-dimensional (3-D) Cartesian coordinates are rectangular parallelepipeds and therefore have rectangular cross sections in any planes parallel to any pair of axes. The computational grid cells in 2-D cylindrical coordinates are toroidal rings with rectangular cross sections. All 2-D and 3-D axes are orthogonal. One-dimensional (1-D) rectangular, cylindrical, and spherical coordinate systems can also be modeled. The reader is referred to the appropriate users' manuals for practical information about the structure and use of the CTHGEN[6] grid generation code, the CTH[7] hydrocode, and their supporting utilities.

It was noted previously[1] that, ideally, a meaningful subsection of a postulated munitions storage area should be modeled in a 3-D Cartesian computational grid. With such a grid design, most of the first-order physics of the system could be modeled. Logic was then presented to support the choice of performing these early computations using simplified representations of the munitions stacks and barricades in a 2-D Cartesian coordinates system. The five computations presented here use the same gridding and representations of the munitions stacks and barricades as were used in Computations 970908 and 971001 reported previously. The nominal computational cell dimensions are 4.0 cm in both Δx and Δy, which are large for shock and detonation front resolution, but a compromise out of necessity because of the long time and large space being simulated. These computations were performed on the Silicon Graphics, Inc., (SGI) Origin 2000 unclassified computers at the ARL Major Shared Resource Center (MSRC) at Aberdeen Proving Ground (APG), MD. This is one of four MSRCs in the United States that are administered by the High Performance Computing Modernization Office (HPCMO). Each of these 2-D Cartesian computations took about 250,000 central-processor-unit (cpu) seconds.

The donor stack is modeled as an uncased charge with no packing materials. This reduced the analysis to one of blast loading only, with no production of fragments or other debris. The explosive mass of the donor stack is modeled as a single, condensed charge rather than as a distributed set of smaller condensed charges. The choice of 2-D Cartesian coordinates meant that the computations provided a worst-case blast loading (i.e., conservatively high) on the barricade for the simplified, uncased charge of condensed high explosives by eliminating the possibility of having any compression or expansion waves in the direction of depth of the munitions stacks and barricade. (Depth is a measure parallel to both the ground and the side walls of the munitions stack, and normal to the page in the flow field plots shown later.) In effect, the donor and acceptor stacks and the barricade have an infinite depth in that coordinate system. In the CTH hydrocode model, which uses the centimeter-gram-second (cgs) units system, this implies a unit depth of 1.0 cm. This also means that even though the following section describes the location of the central detonation initiation "point," in the chosen 2-D Cartesian coordinates system, the detonation is actually being modeled as simultaneous along an infinite central line. The air blast loading, especially the peak, on the acceptor stack may not necessarily be conservatively high in this 2-D system compared with what might be computed in a 3-D system. In a 3-D system, a blast wave will diffract both over and around an object, so a strong shock can be regenerated more quickly on the lee side of the object. The impact loading of the barricade on the acceptor stack is almost certainly conservatively high in the 2-D system and is responsible for most of the impulse delivered to the acceptor stack.

2.2. The Donor Munitions Stack

The choice of the munitions in the donor munitions stack was made by consulting a previous ARL report on fragment propagation probabilities by Starkenberg et al.[8] Part

of that study used palletized and single M107 155-mm projectiles as fragment donors to analyze the threat to palletized Tube-Launched Optically Tracked Wire-Guided (TOW-2A) missiles as acceptor munitions. The donor munitions stack for both the previous and the current studies was assumed be of the same size as one consisting of 72 pallets of M107 155-mm projectiles, stacked three pallets high by four wide by six deep. Each pallet contains eight rounds. The dimensions of this particular stack are 2.44 m high by 2.94 m wide by 2.19 m deep (8.00 ft by 9.63 ft by 7.20 ft). A single M107 round can contain either 6.62 kg (14.6 lbm, where "lbm" denotes pounds mass, avoirdupois) of TNT or 6.98 kg (15.4 lbm) of Composition-B (hereinafter referred to as "Comp-B"). The total mass of a pallet, including packaging, is 362 kg (797 lbm).[9] Thus, a presumed stack of M107 munitions would contain 576 rounds, having a total mass of Comp-B equal to 4,024 kg (8,870 lbm). For simplicity, the nominal explosive mass of Comp-B for this computational study was taken as 4,000 kg (8,818 lbm) for the donor stack, which is the regulatory maximum.[10] The total mass of an actual stack containing 72 pallets of M107 rounds is 26,029 kg (57,384 lbm), including all packaging materials. This equates to a mass of 118.61 kg/cm of depth for the actual stack with all materials. The acceptor stack was assumed to be of the same physical dimensions and total mass as those of the donor stack.

Just as in Computation 970908, it was decided to model the donor stack as an uncased explosive charge. The explosive modeled was Comp-B, taken at its reference density of 1.72 g/cm^3 in its undetonated state, and modeled[11] within the Sesame[12] equation-of-state (EOS) package. The SNL Sesame EOS package includes tabular data for high explosives and separate implementations of data for the Mie-Gruneisen, Jones-Wilkins-Lee (JWL), and ideal-gas EOSs. The explosive charge was placed within the computational flow field with its center coincident with that of the M107 donor stack described before. After assigning the donor stack the nominal explosive mass of 4,000 kg and using the actual stack depth of 2.19 m, this equated to an explosive charge mass of approximately 18.227 kg/cm of depth of the stack to be modeled in the unit-depth 2-D Cartesian coordinates flow field in CTH. This mass of Comp-B was modeled as a rectangle whose width and height are in direct proportion to those for the donor stack. Specifically, the explosive charge was 93.91 cm high and 113.04 cm wide (i.e., the full width, and not one-half width for symmetry), located with its center of mass 121.92 cm above the ground plane. The ground plane was designated as a frictionless, perfectly reflective boundary.

A small central section of the explosive charge, half of which was placed at the left symmetry boundary, served as a computational "booster" charge. It was detonated using the programmed burn[6] model using a constant detonation velocity of 7.98 km/s for reference-density Comp-B.[13] This model simulates the complete detonation of any part of an explosive charge that is passed by the expanding theoretical detonation front moving at that constant velocity. The remainder of the detonation was modeled using the "history variable reaction burn" (HVRB) model.[12] The HVRB model evaluates the thermodynamic state of a mass of undetonated explosive in a given computational flow field cells to determine if that material

should be detonated in that time step. The detonation initiation point was located at the center of the explosive charge at the (X,Y) point (0.0, 121.92 cm).

2.3. The Barricade

The barricade shape chosen for the computations is identical to that used in Computations 970908 and 971001 and similar to that being provided for evaluation by a Small Business Innovative Research (SBIR) contractor.[14] That design consists of a pyramidal stacking of a number of identical, cylindrical, water-filled tubes. The computational study presented in this report is simply an evaluation of that type of generic design and should not be construed as either a direct criticism or endorsement of any particular design by the contractor. For simplicity in these computations, it is assumed that the stacking results in a shape that has a continuous sloping side with an inside angle, θ, at the top that is equal to 30 degrees when measured from a line perpendicular to the ground plane. An idealized trapezoidal cross section that has no internal air spaces and consists only of water is assumed. The materials that comprise the tubes' walls are ignored. The height of the barricade, H, is 243.84 cm (8.0 ft), as stated in the contract. The width of the barricade at the flat top, W_t, is assumed for the purposes of this computational study as 1.0 m (3.28 ft). The width of the barricade at the base, W_b, is then $W_b = W_t + 2H\tan(\theta)$, or 381.56 cm (12.52 ft) for this geometry. The mass of water for the barricade is 58.71 kg/cm of depth. The water in the barricade was modeled using the CTH Sesame EOS for water.[15] The bottom corner of the barricade closest to the donor stack was placed at the defined standoff distance, which varied from 3.05 m (10 ft) to 2.00 m (6.56 ft), from the nearest side of the donor stack. The standoff distance here is measured from the face of what would have been the actual side of the donor munitions stack, not the condensed explosive charge representing the stack.

2.4. The Acceptor Munitions Stack

The acceptor munitions stack was modeled in all computations as a simple, relatively inert mass of iron[16] with the same height (2.44 m) and width (2.94 m) as the reference M107 munitions stack. The acceptor stack in each computation was located at a standoff distance equal to that between the donor stack and the barricade. The purpose in modeling the acceptor stack as a full-sized mass of iron was for the convenience of having a massive, relatively non-responding object with the correct physical dimensions in order to observe wave interactions on the surface and to provide surface blast loading data through the use of CTH's "tracer" particles placed in the air near the surfaces. Tracer particles are massless points that are specified at desired locations by the user at grid generation time. They may be fixed in computational space or be free to move along one or more of the principal axes in the grid. A relatively full complement of data describing the thermodynamic state and other physical parameters at the location of each tracer is recorded for later processing by the user. When analyzing the whole-body response of the acceptor stack later in this report, the

correct (i.e., 118.61 kg/cm of depth) acceptor stack mass was used to compute the motion of the acceptor stack from the X-direction momentum of the massive iron stack. Some of the details of the blast development in this computational series and subsequent interactions between the blast and the barricade and then the barricade and the acceptor stack are surely artifices of the simplified geometries, but the overall dynamics appear to be quite reasonable.

3. THE HYDROCODE COMPUTATIONS

3.1. Flow Field Development

Computation 980505 simulated a fully coupled blast and impact loading sequence at a standoff of 3.05 m (10.0 ft). Because of the trapezoidal cross section, this placed the center of mass of the barricade at a nominal X distance of 4.96 m (more precisely, 495.58 cm) from the true right face of the donor stack. Computation 980505 thereby allows a direct comparison with the previously reported[1] uncoupled pair of computations. Figure 1 shows the computational flow field at the start of Computation 980505 at the instant of the initiation of the detonation (hereinafter referred to as "initiation") with time defined to be equal to zero. The "Y" axis at the left of the figure represents the height measured from the ground plane. In this simple 2-D Cartesian coordinate system, the left boundary at the Y axis is designated as a frictionless, perfectly reflective plane of symmetry. The "X" axis represents the measure of width in the system and coincides with the frictionless, perfectly reflective ground plane. The Y axis at the X = 0.0 location is also a vertical bisector of the donor stack. The air in the flow field, modeled with data from Graboske[17] within the Sesame[12] EOS package, is shown with the color yellow. The top and right transmissive boundaries are marked by the top and right edges of that yellow region. These transmissive boundaries were designated as zero-gradient, outflow-only boundaries to minimize the possibilities of generating spurious, mathematically generated inflows when those boundaries are struck by large-gradient outflows. The explosive charge representing the donor stack is shown as the red (one-half) rectangle on the left symmetry boundary, the water barricade is shown as the blue trapezoid, and the acceptor stack is shown as the black rectangle (the object closest to the right transmissive boundary).

Figure 2 shows the computational flow field at 2.5 ms after the initiation of the donor stack. This initial sequence of flow field plots is presented at closely spaced time intervals to illustrate an interesting fluid dynamic wave that develops at the bottom of the right face of the barricade and becomes increasingly more pronounced as it moves up that face as time progresses. While this wave would probably not develop in a multi-walled water barricade with the same overall cross section, it is important to at least understand its origin and development because water from it makes the first significant contact with the acceptor stack in these computations. The detonation process had already been completed by this time (theoretically at 0.092 ms). The expanding explosive products and leading shock have

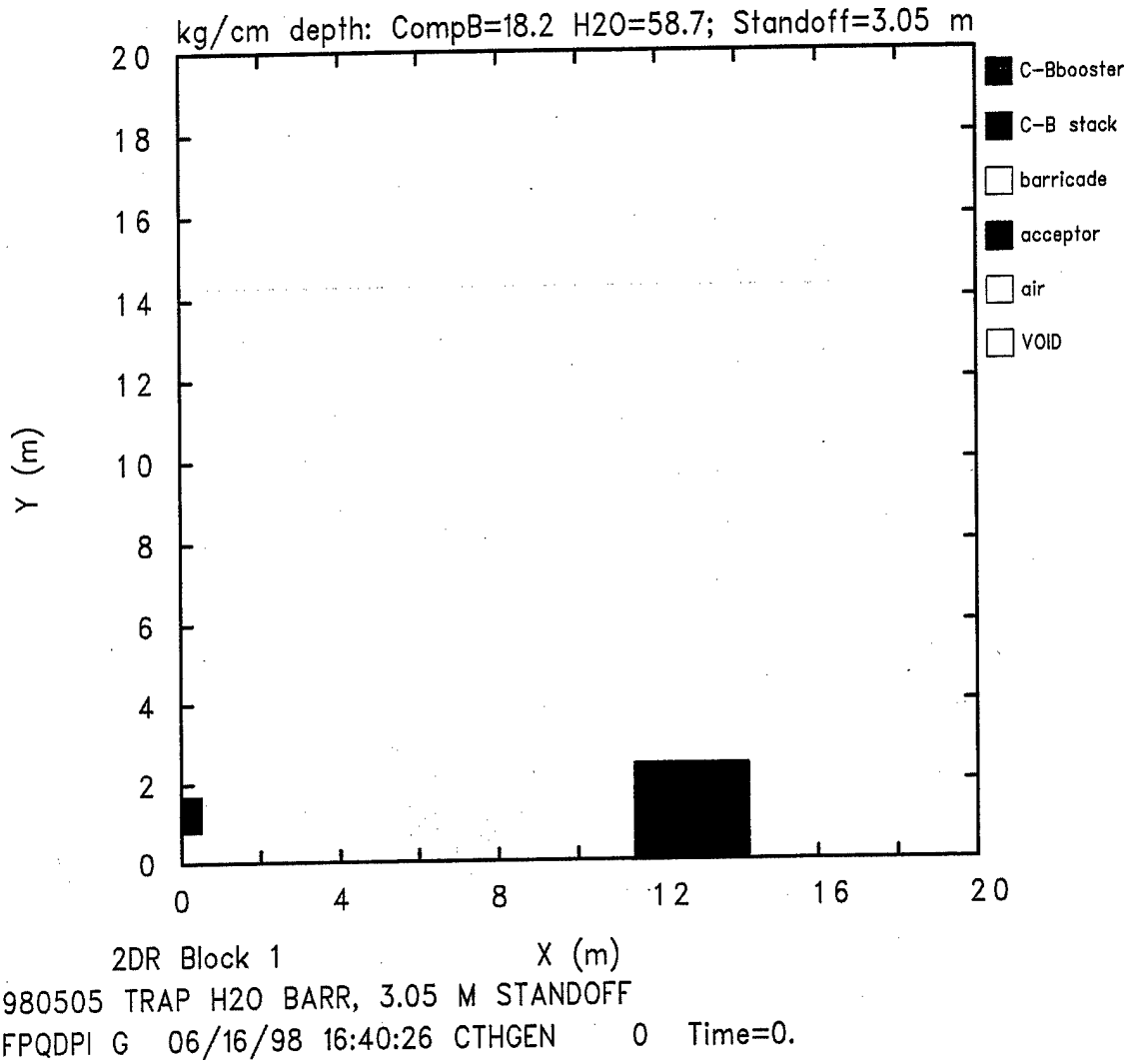

Figure 1. Flow Field at Time = 0.0 for Computation 980505, 3.05-m Standoff.

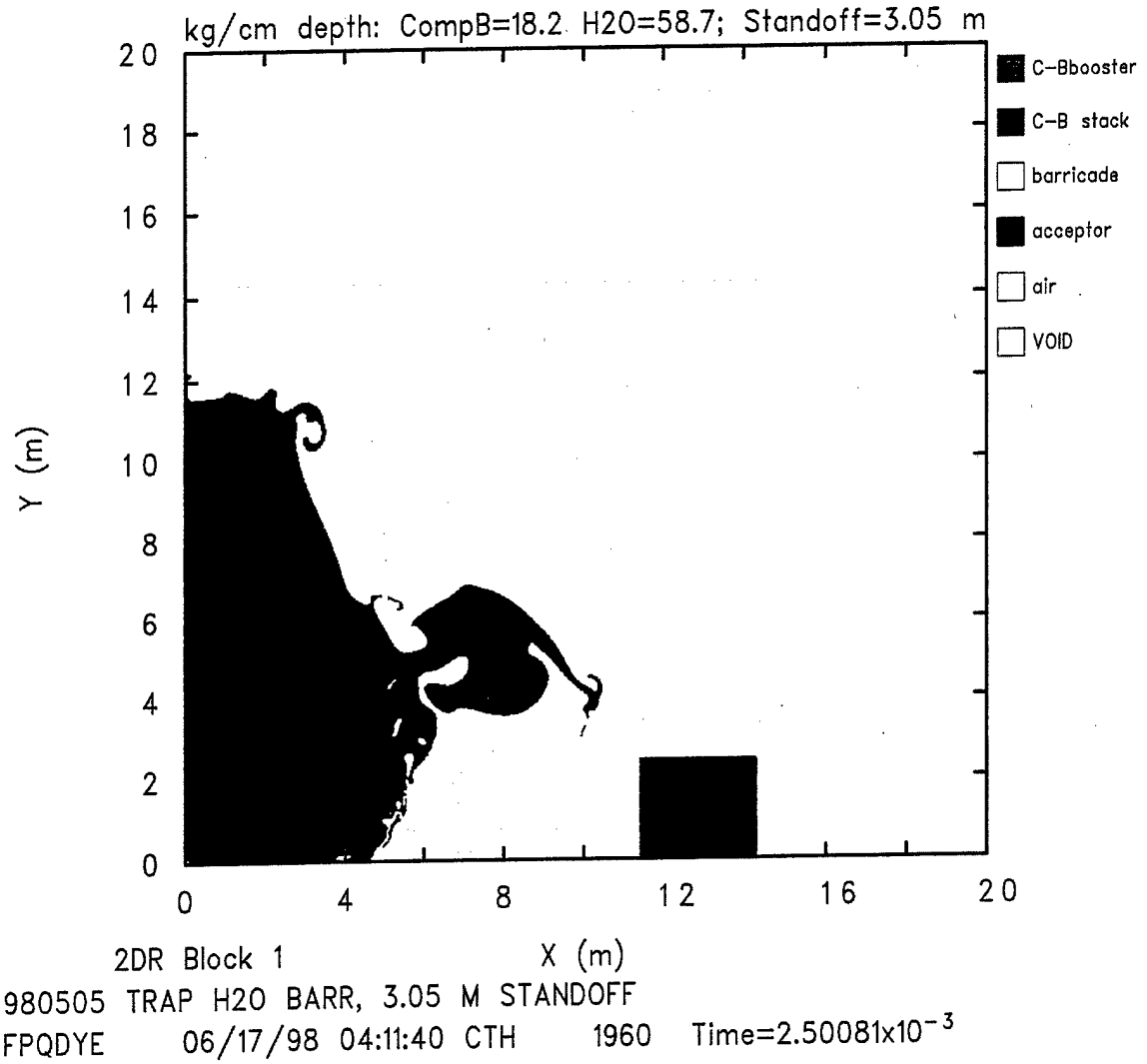

Figure 2. Flow Field at Time = 2.5 ms for Computation 980505, 3.05-m Standoff.

just begun to deform the barricade, with some water already separating from the top of the barricade. The shock front has already diffracted over the top of the barricade and has a distorted, trailing region of explosive products that has not yet reached the plane of the left face of the acceptor stack. There has as yet been no significant distortion of the right face of the barricade.

Figure 3 shows the computational flow field at 5.0 ms after the initiation of the donor stack. The first region of expanding explosive products and the leading shock have already traveled past and mostly above the acceptor. The thinner top section of the water barricade has deformed both upward and toward the acceptor stack on an apparent trajectory that will take most of it over and away from the acceptor stack. The lower and central regions of the barricade are now beginning to bulge toward the acceptor stack. The beginning of the wave on the right face of the barricade that was referred to previously can be seen as the cusp-like feature at about the (X=9.0, Y=0.75 cm) point.

Figure 4 shows the computational flow field at 7.5 ms after the initiation of the donor stack. The expanding explosive products are now widespread, including being above the acceptor stack but with no indications of impingement on it. The overall distortion of the barricade is continuing. Some parts of the top section of the barricade are now passing 1 to 2 m above the top of the acceptor stack. The wave on the right face of the barricade is continuing to grow, move upward, and show more extension rightward.

Figure 5 shows the computational flow field at 10.0 ms after the initiation of the donor stack. The wave on the right face of the barricade is continuing to grow, move upward, and even show signs of "breaking" in a manner roughly analogous to a solitary wave on a shallow, rising shore, but gravitational forces have not been included in these computations. The driving forces behind this wave appear to be a combination of upward and rightward flow of water from the middle and possibly lower sections of the barricade as it moves past slower, more rightward internal regions of water, plus possibly some external supporting force from reflected air flow from the left face of the acceptor stack, and possibly from the simplified representation of the detonation of the donor stack. As of this time, no part of the barricade appears to have arrived at the left face of the acceptor stack, nor have any explosive products.

Figure 6 shows the computational flow field at 12.5 ms, with further distortion and translation of the barricade and further development of the wave on the right face of the barricade. Figure 7 shows the computational flow field at 15.0 ms, with the leading edge of the wave on the right face of the barricade just about to impact upon the top-left face of the acceptor stack. This will be the first significant contact of water from the barricade with the acceptor stack. The remainder of the lower sections of the barricade, which will ultimately deliver the greatest impact on the acceptor stack left face, is moving toward the acceptor stack but is several milliseconds away from impact.

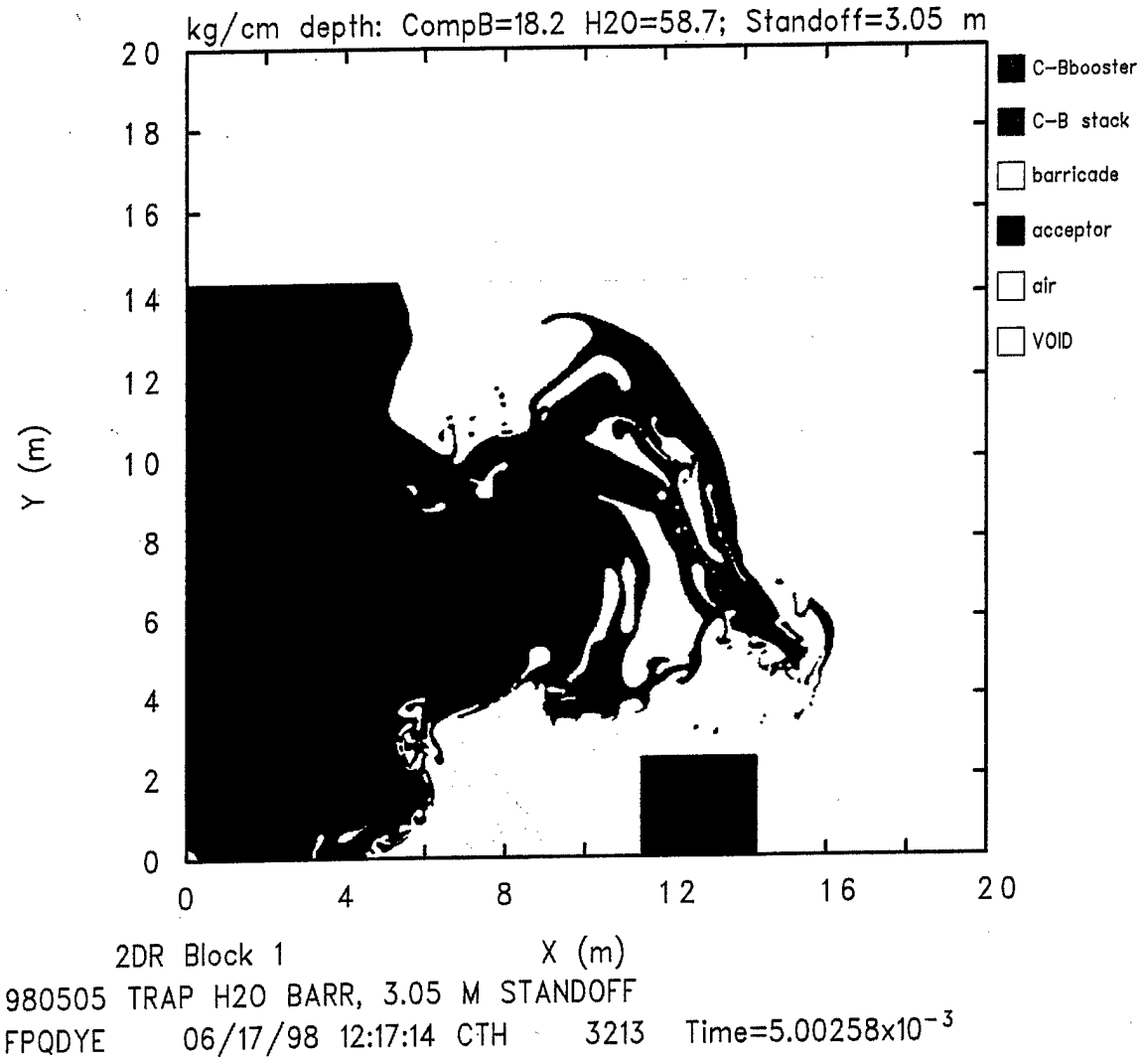

Figure 3. Flow Field at Time = 5.0 ms for Computation 980505, 3.05-m Standoff.

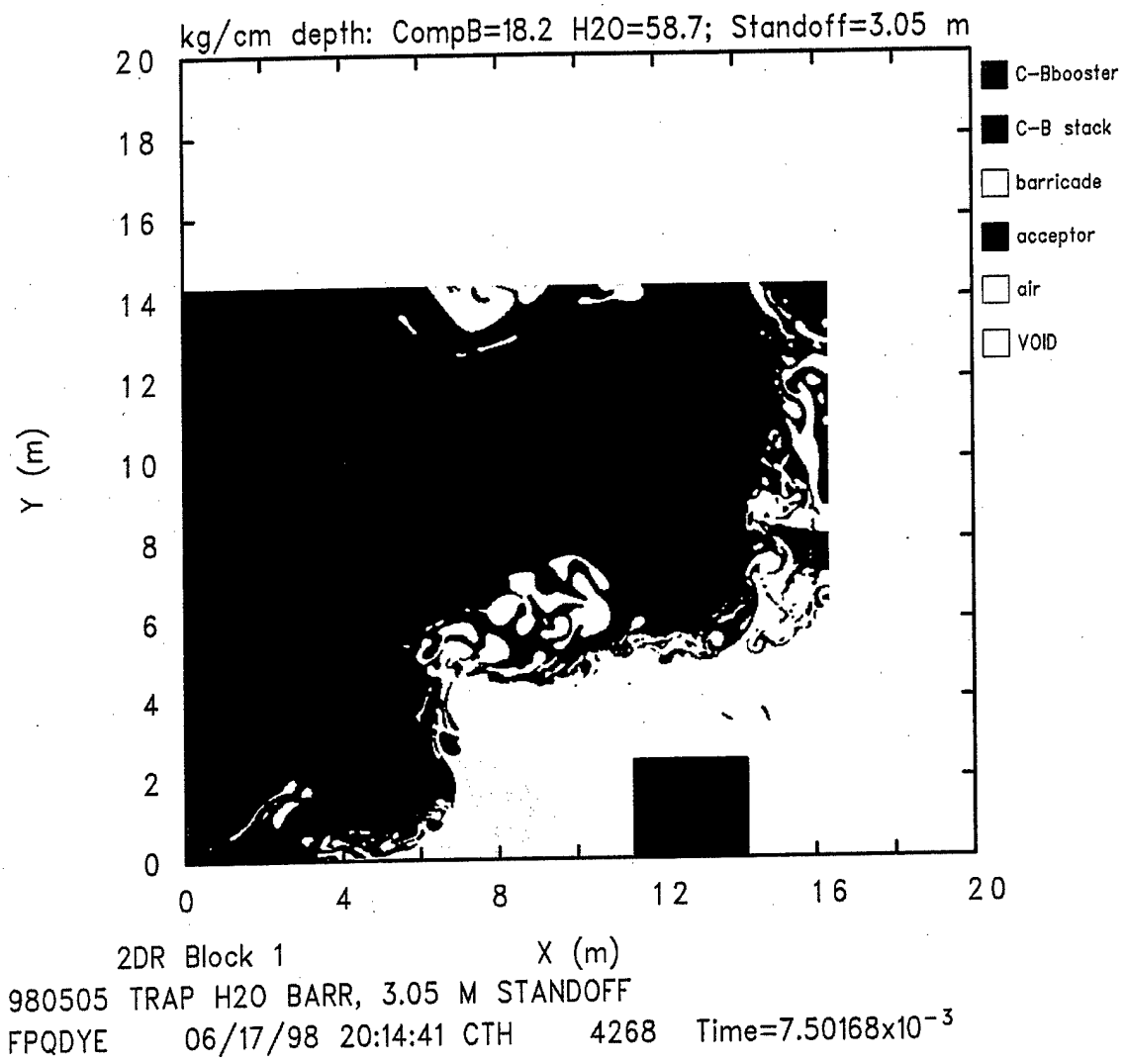

Figure 4. Flow Field at Time = 7.5 ms for Computation 980505, 3.05-m Standoff.

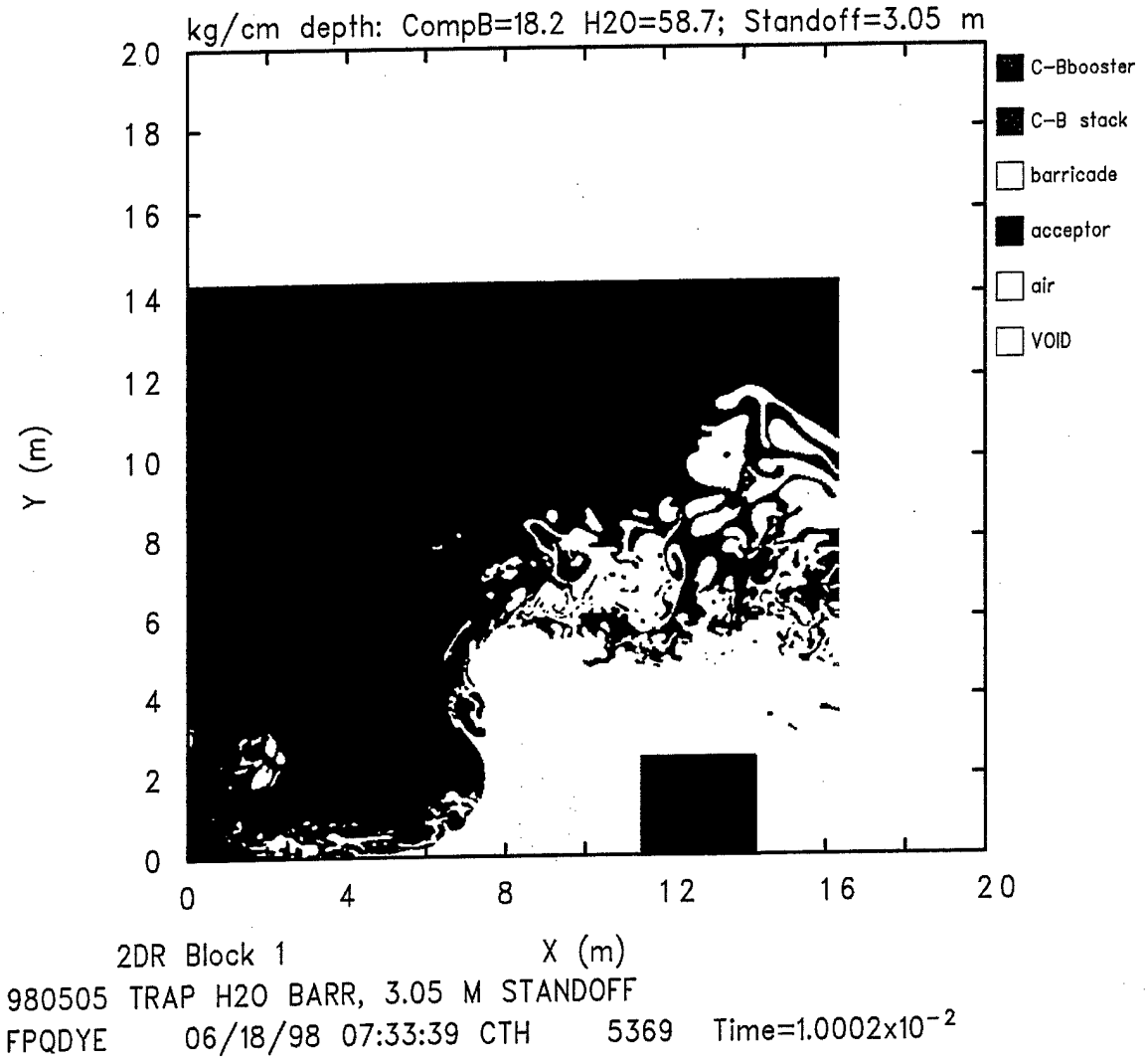

Figure 5. Flow Field at Time = 10.0 ms for Computation 980505, 3.05-m Standoff.

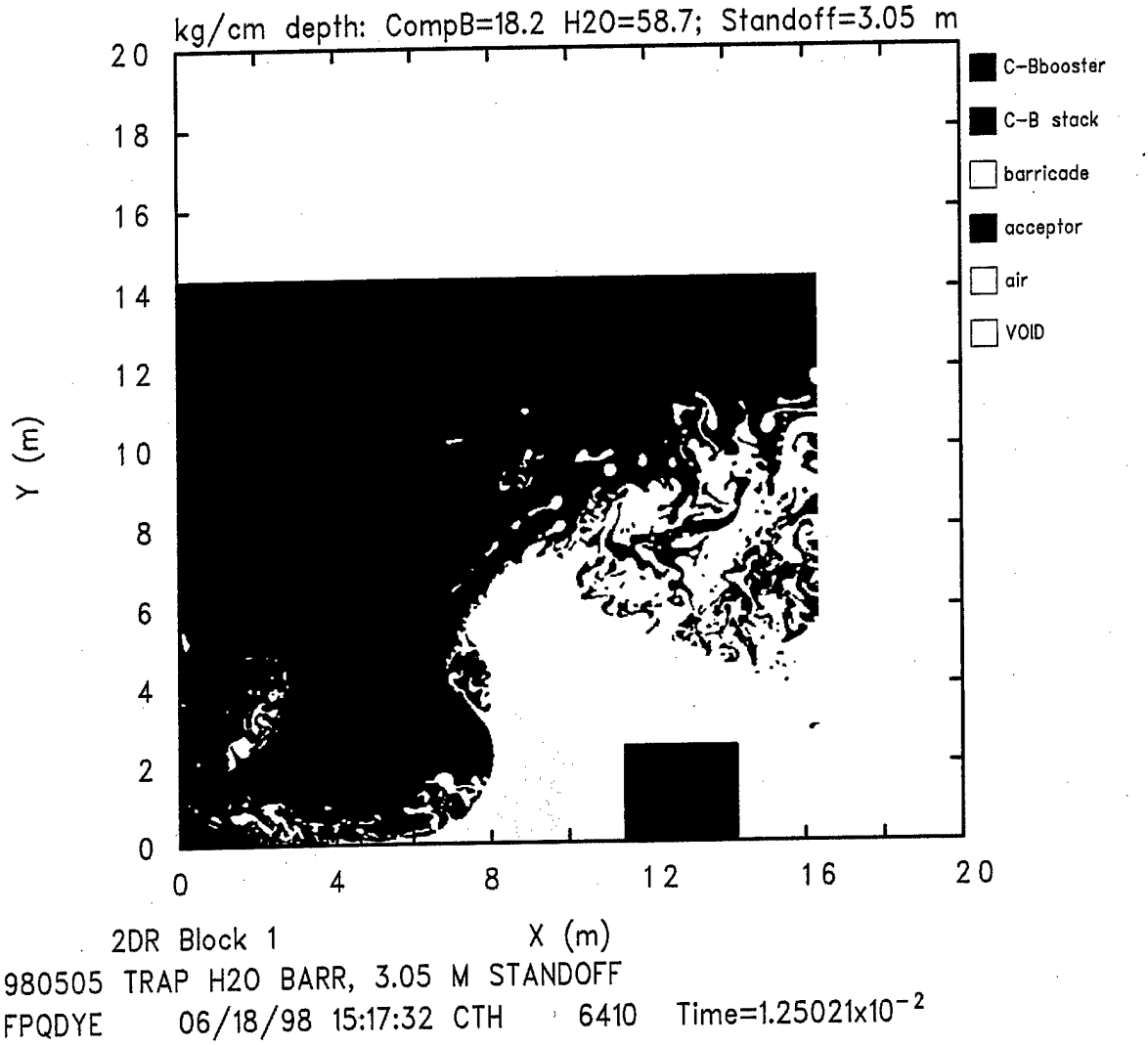

Figure 6. Flow Field at Time = 12.5 ms for Computation 980505, 3.05-m Standoff.

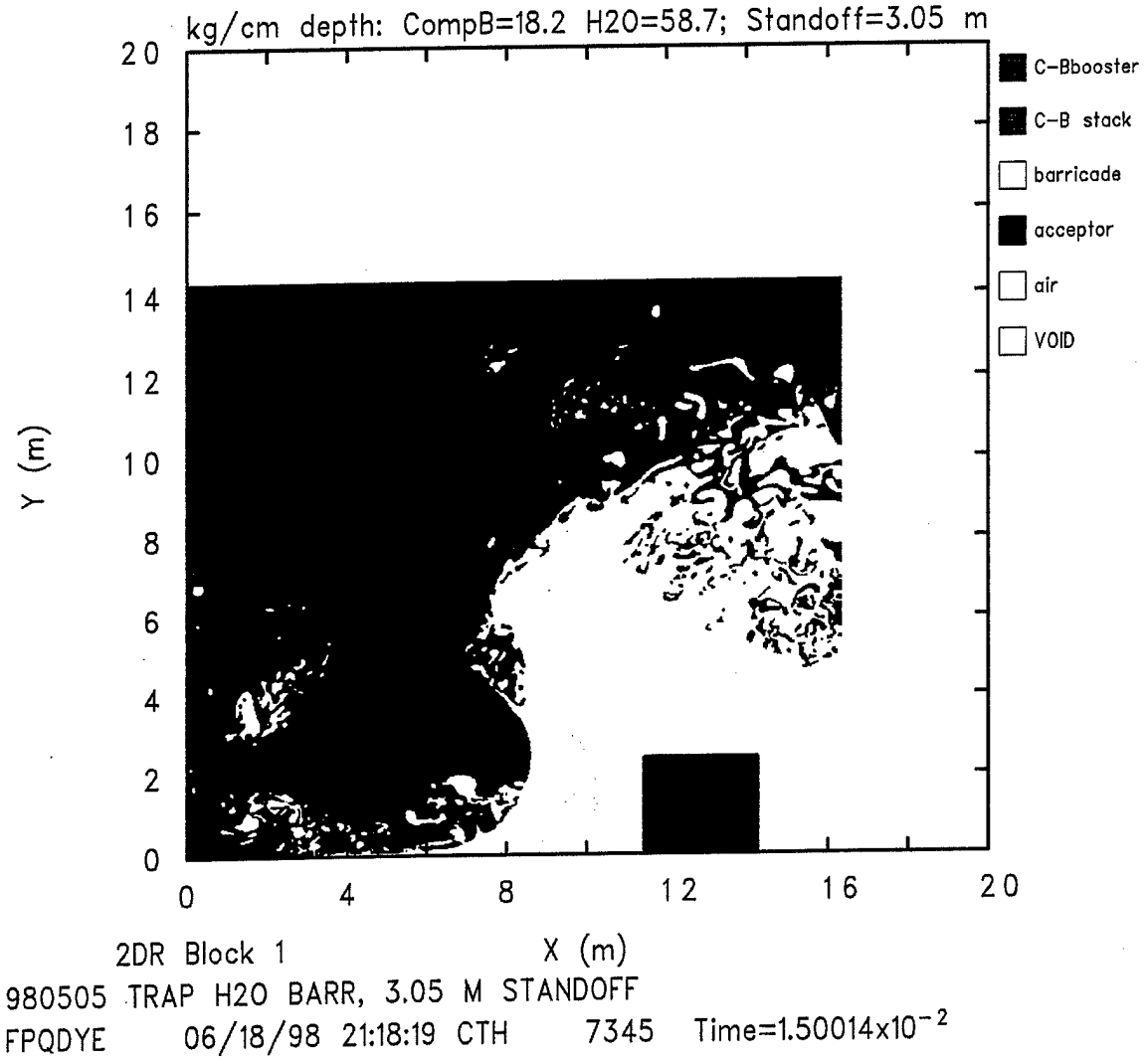

Figure 7. Flow Field at Time = 15.0 ms for Computation 980505, 3.05-m Standoff.

Figure 8 shows the computational flow field at 20.0 ms after initiation. The water from the wave on the right face of the barricade has begun its interaction with the top of the left face of the acceptor stack. The lower part of the barricade is still moving toward the acceptor stack. A region of air has been trapped against the lower left face of the acceptor stack and is providing some relatively minor loading to the acceptor stack at this time. Most of the air blast and virtually all of the explosive products have been deflected upward and away from the acceptor stack.

Progressing further in time, Figure 9 shows the computational flow field at 30.0 ms after initiation. The main body of the barricade is interacting with the left face of the acceptor stack around this time. A significant portion of the barricade is passing over and above the top of the acceptor stack, contributing no loading to it. Most of the loading on and acceleration of the acceptor stack occurs during the several milliseconds around this time. However, the shape of the barricade has caused the loading on the acceptor stack to be delivered in a multi-stage process, thereby reducing the peak values of both the loading and response of the acceptor stack. This is quantified later in this report.

Finally, Figure 10 shows the computational flow field at 40.0 ms after initiation. The interaction of the lower section of the barricade with the lower left face of the acceptor stack has been completed, and much of the water is moving in the negative X direction in a rebound stage. There is still some water in contact with the upper left face of the acceptor stack, but the loading on the stack is relatively small. There has still been no contact of explosive products with the acceptor stack indicated in this computation, which was stopped at this point.

Computation 980507 simulated a standoff distance of 2.75 m. It was run for the same amount of simulated time, 40.0 ms, as was done for Computation 980505 and used the same computational gridding with the same munitions stack and barricade geometry. The temporal sequence of flow field material plots shows qualitatively similar behavior to that for 980505, with impact times occurring sooner because of the reduced standoff distance. For the sake of brevity, these are not shown. Computation 980521 simulated a standoff distance of 2.50 m. Figure 11 shows the computational flow field at time = 0.0, the instant of initiation of the donor stack. Except for the standoff distance, the computational flow field, the munitions stacks, and the barricade are identical to those for 980505 (see Figure 1) and 980507.

Figure 12 shows the computational flow field at time = 10.0 ms for Computation 980521. This shows qualitatively similar behavior to that shown in Figure 5 for 980505, except that the barricade is closer in space and time to its initial contact with the acceptor stack left face. Figure 13 shows the flow field at 20.0 ms after initiation. A comparison with Figure 8 shows that 980521 has a larger area of water interaction at the top of the left face of the acceptor stack and a more compressed region of air at the base. Figure 14 shows the flow field at 30.0 ms for 980521 and Figure 15 shows the flow field at 40.0 ms, each comparable to the respective times for 980505 but with events happening more quickly for the closer

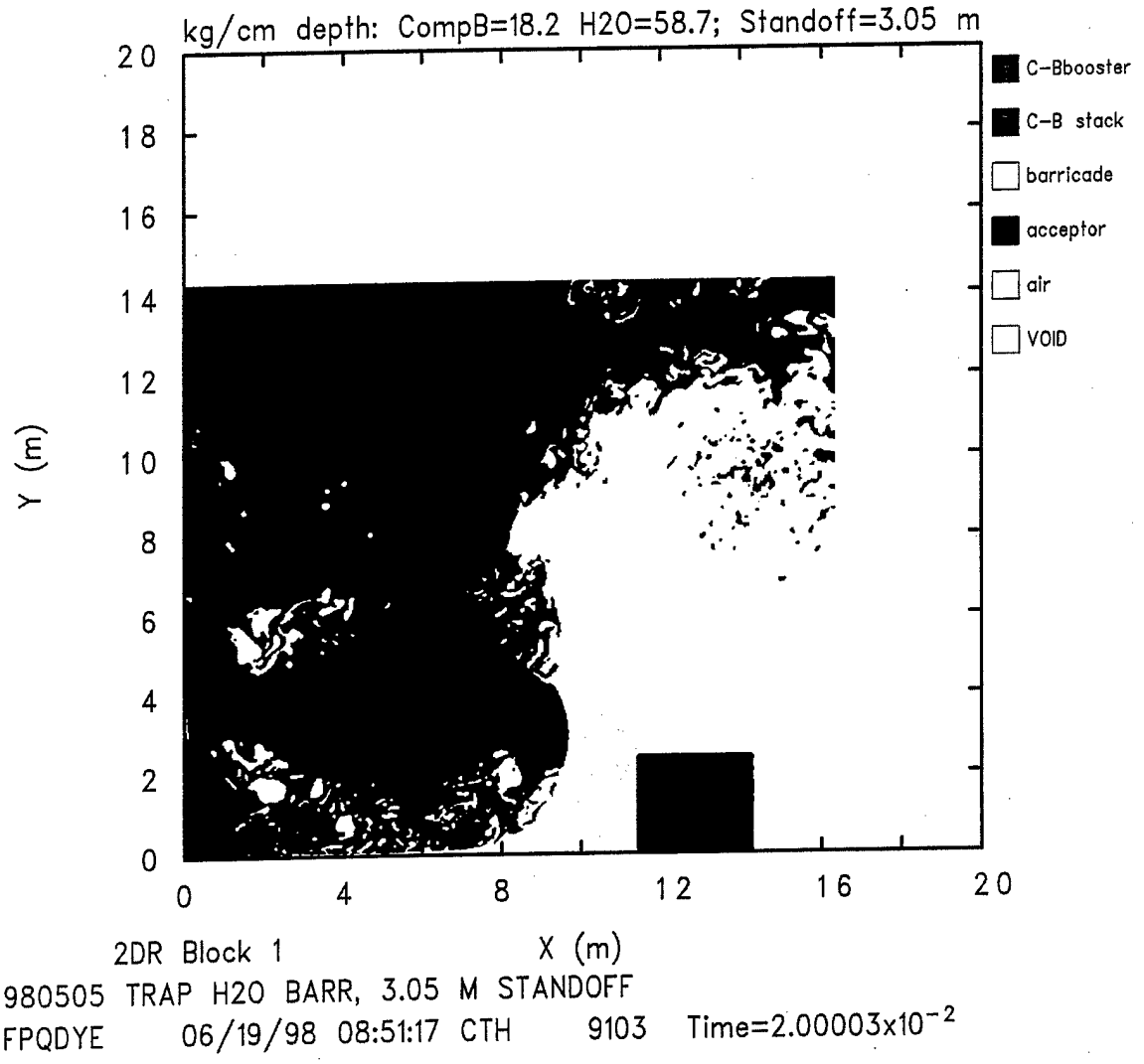

Figure 8. Flow Field at Time = 20.0 ms for Computation 980505, 3.05-m Standoff.

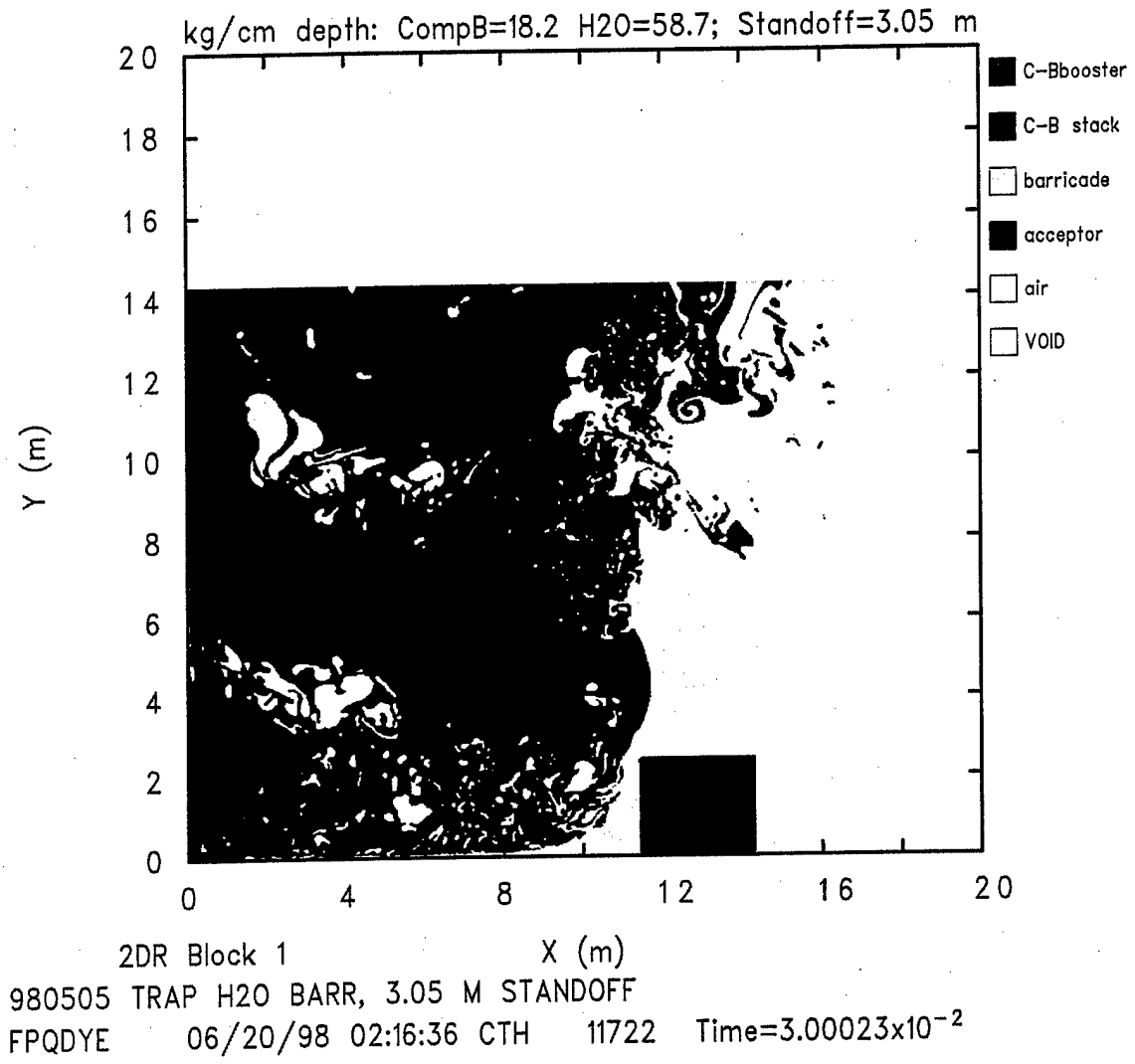

Figure 9. Flow Field at Time = 30.0 ms for Computation 980505, 3.05-m Standoff.

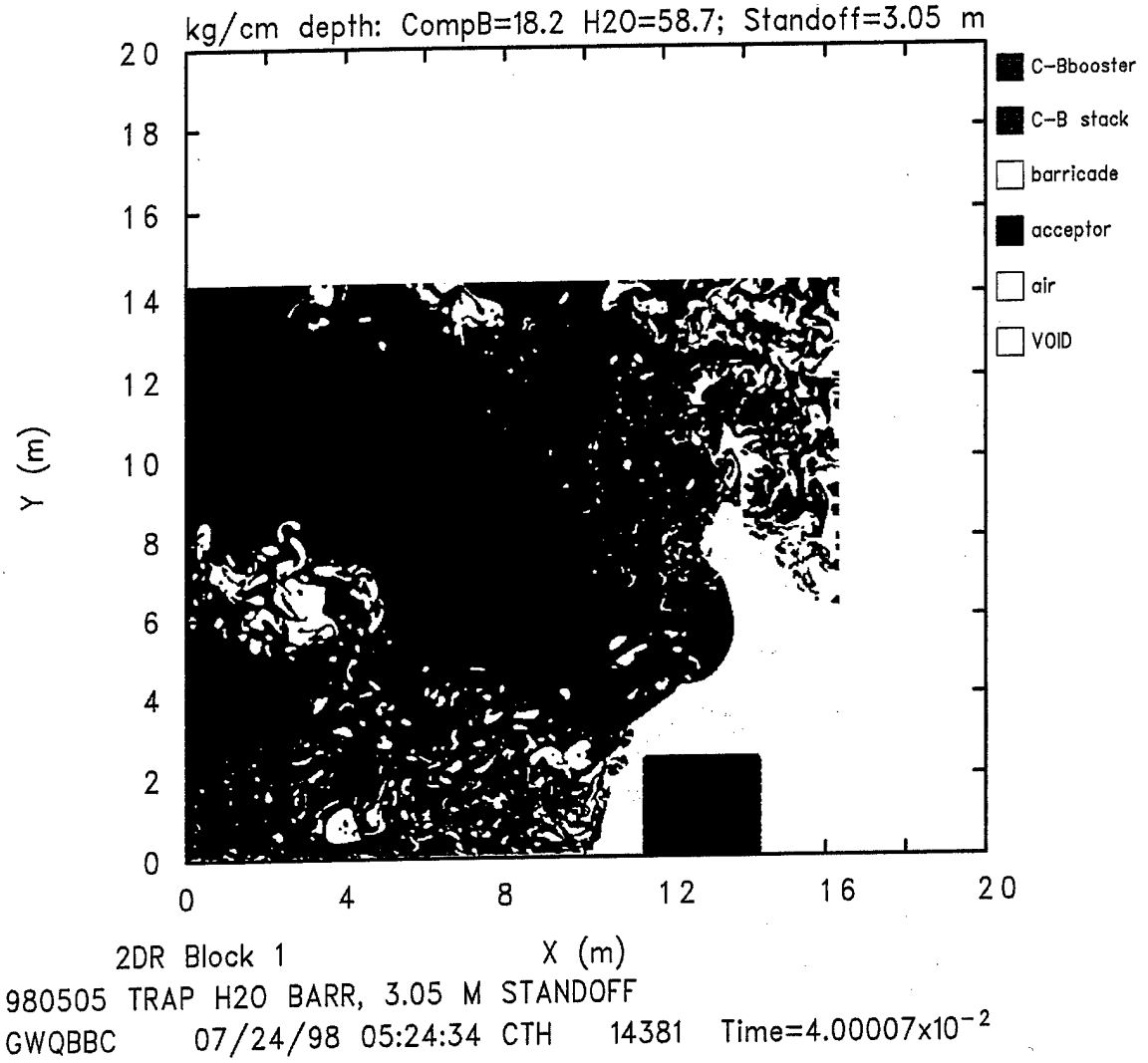

Figure 10. Flow Field at Time = 40.0 ms for Computation 980505, 3.05-m Standoff.

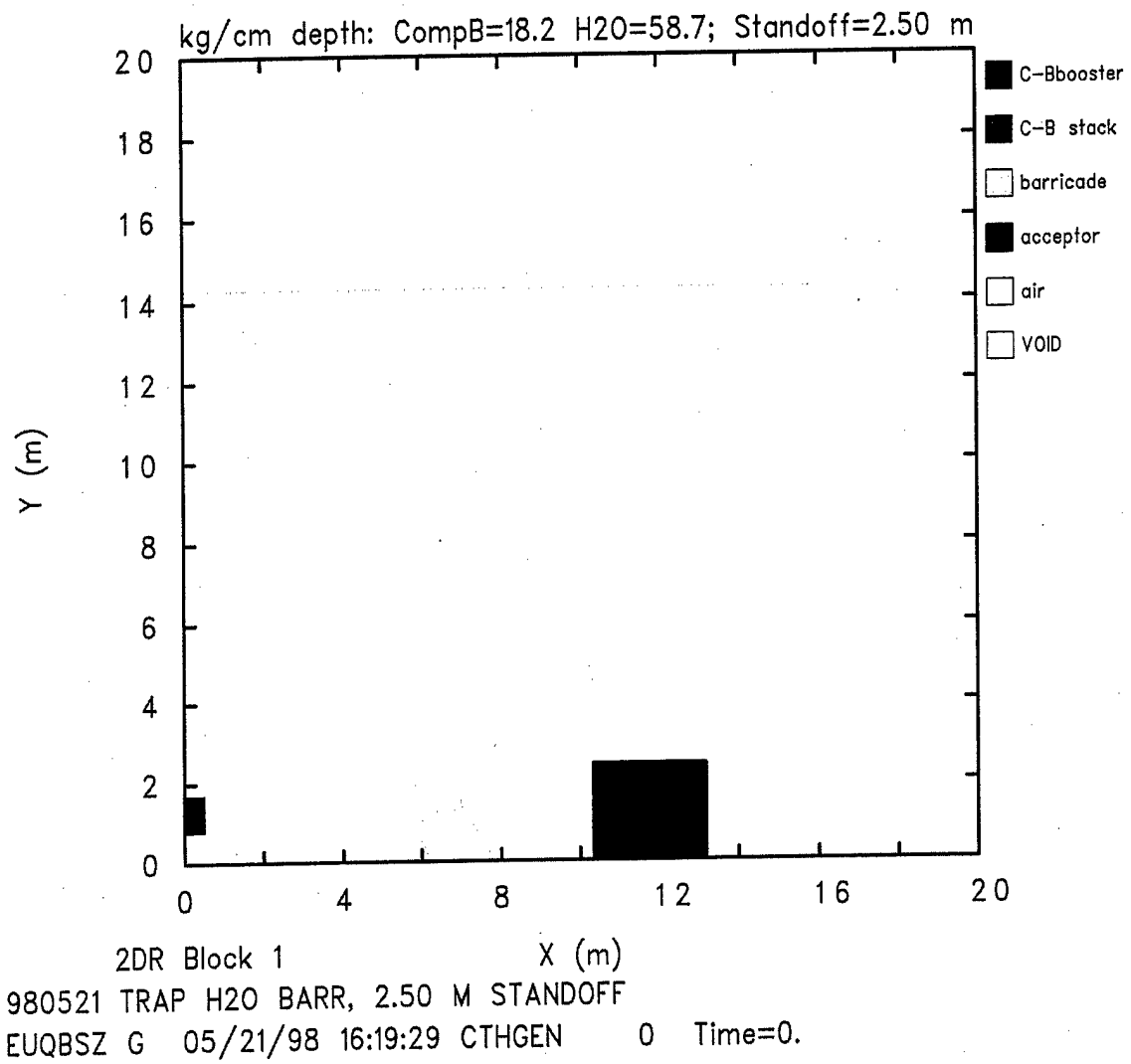

Figure 11. Flow Field at Time = 0.0 for Computation 980521, 2.50-m Standoff.

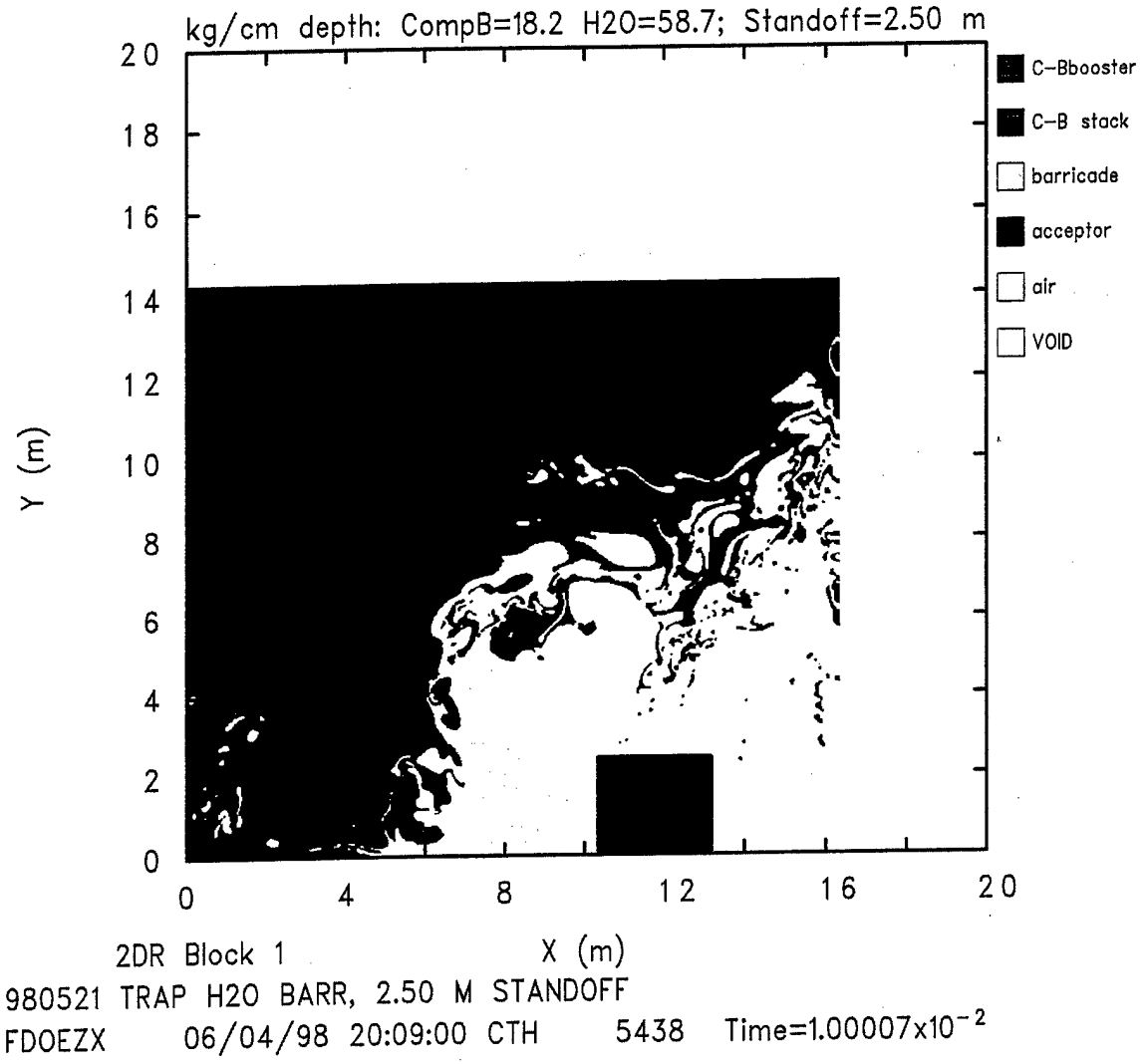

Figure 12. Flow Field at Time = 10.0 ms for Computation 980521, 2.50-m Standoff.

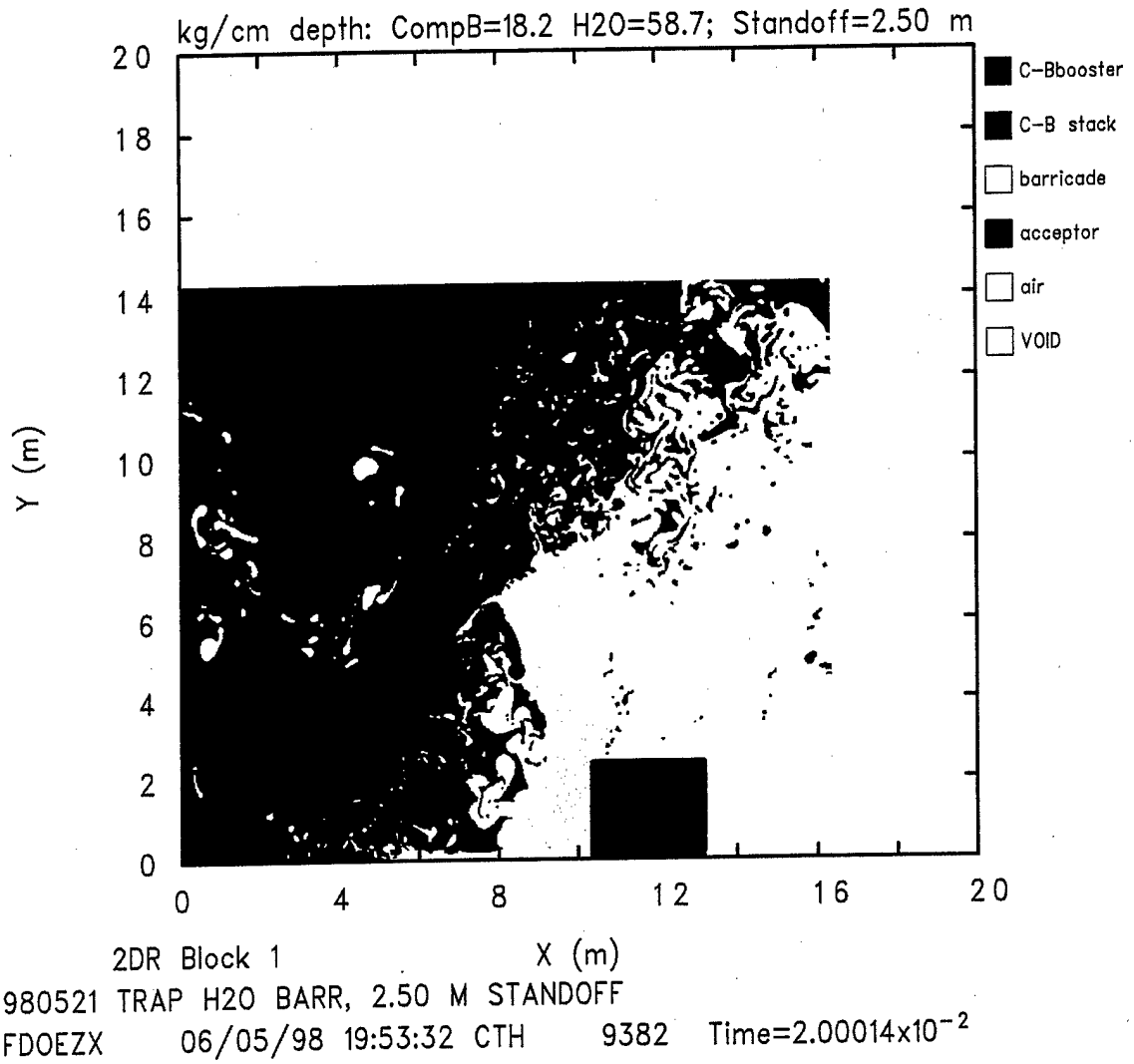

Figure 13. Flow Field at Time = 20.0 ms for Computation 980521, 2.50-m Standoff.

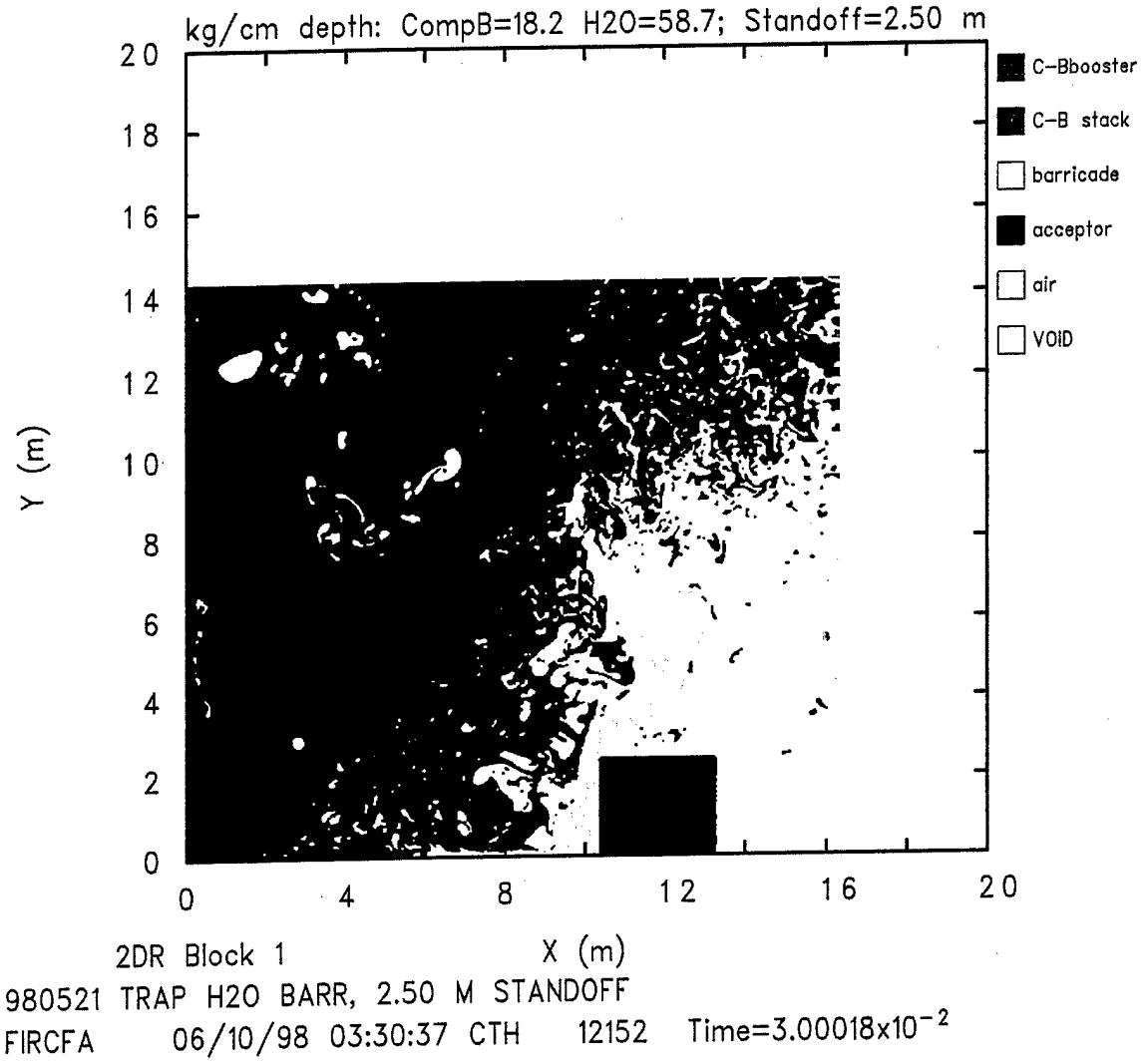

Figure 14. Flow Field at Time = 30.0 ms for Computation 980521, 2.50-m Standoff.

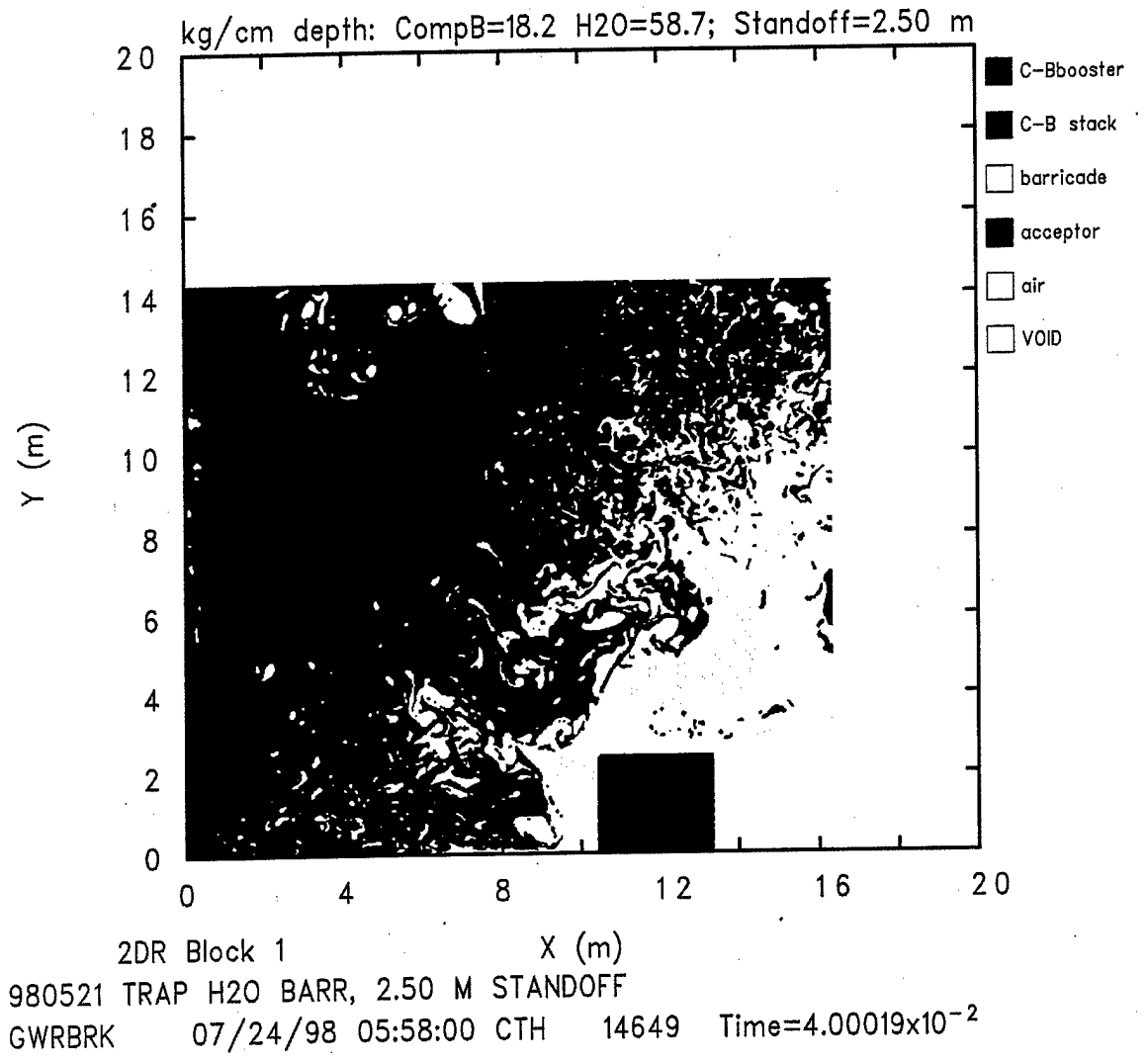

Figure 15. Flow Field at Time = 40.0 ms for Computation 980521, 2.50-m Standoff.

standoff in 980521. As was the case for Computation 980505, Figures 11 through 15 show that there has been no explosive products contact with the acceptor stack through 40 ms.

Computation 980528 simulated a standoff distance of 2.25 m and was also run to a simulated time of 40.0 ms, using the same computational gridding with the same munitions stack and barricade geometry as for all other computations in this series. The temporal sequence of flow field material plots shows qualitatively intermediate behavior between that for 980521 and 980610, with impact times occurring sooner than those for 980521 because of the reduced standoff distance. Just as for 980507, these are not shown for the sake of brevity. The last computation in this series, Computation 980610, simulated a standoff distance of 2.00 m. Figure 16 shows the computational flow field at time = 0.0, the instant of initiation of the donor stack. Except for the standoff distance, the computational flow field, the munitions stacks, and the barricade are identical to those for the other computations in this series. A comparison with Figure 1 clearly shows how much closer the layout of the stacks and barricade is in 980610. The bottom-left corner of the barricade is 1.048 m closer to the donor stack than in 980505, the bottom-right corner of the barricade is similarly 1.048 m closer to the acceptor stack, and the acceptor stack in 980610 is therefore 2.096 m closer to the donor stack than in 980505. Note that the overall dimensions of the computational flow field, left boundary to right boundary and bottom boundary to top boundary, are identical in 980505 and 980610, as they are in all computations in this series.

Figure 17 shows the computational flow field at time = 10.0 ms for Computation 980610. This shows that the water from the wave on the right face of the barricade has already impacted the acceptor stack at about 2/3 of the height up its left face, whereas Figure 5 shows that the leading edge of the wave is still about 2 m away from the acceptor stack left face. Figure 17 also shows a much more concave left face at this point in time. Figure 18 shows the flow field at 20.0 ms after initiation. By this time, water from the wave on the right surface of the barricade has already interacted with most of the top 1/3 of the left face of the acceptor stack. A comparison with Figure 8 shows that, in Computation 980505, water from the wave has interacted with only the top-most part of the left face of the acceptor stack. Figure 19 shows the flow field at 30.0 ms for 980610. By this time, the barricade has interacted with the entire left face of the acceptor stack and is now rebounding from it. In 980505, the full interaction has not yet occurred by this time. Finally, Figure 20 shows the flow field for 980610 at 40.0 ms, with the interaction with the acceptor stack effectively ended and most of the mass of water already having translated rightward past the left face of the acceptor stack. Computation 980610 also shows no explosive products contact with the acceptor stack through 40 ms.

3.2. Barricade Dynamics

Figure 21 shows the bulk momentum per centimeter depth of the water barricade in the X direction, with positive momentum in the direction of increasing values of X, moving toward

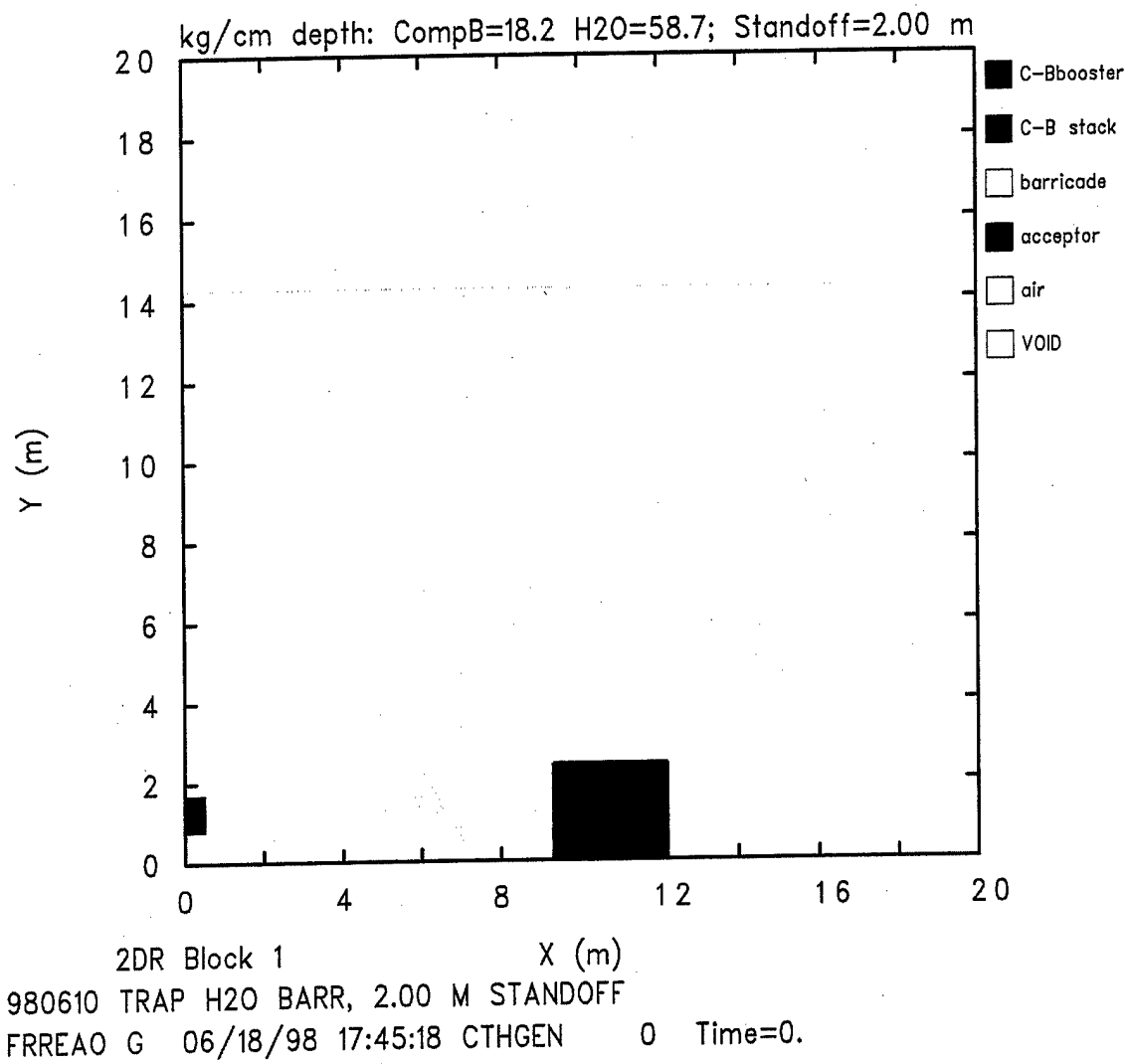

Figure 16. Flow Field at Time = 0.0 for Computation 980610, 2.00-m Standoff.

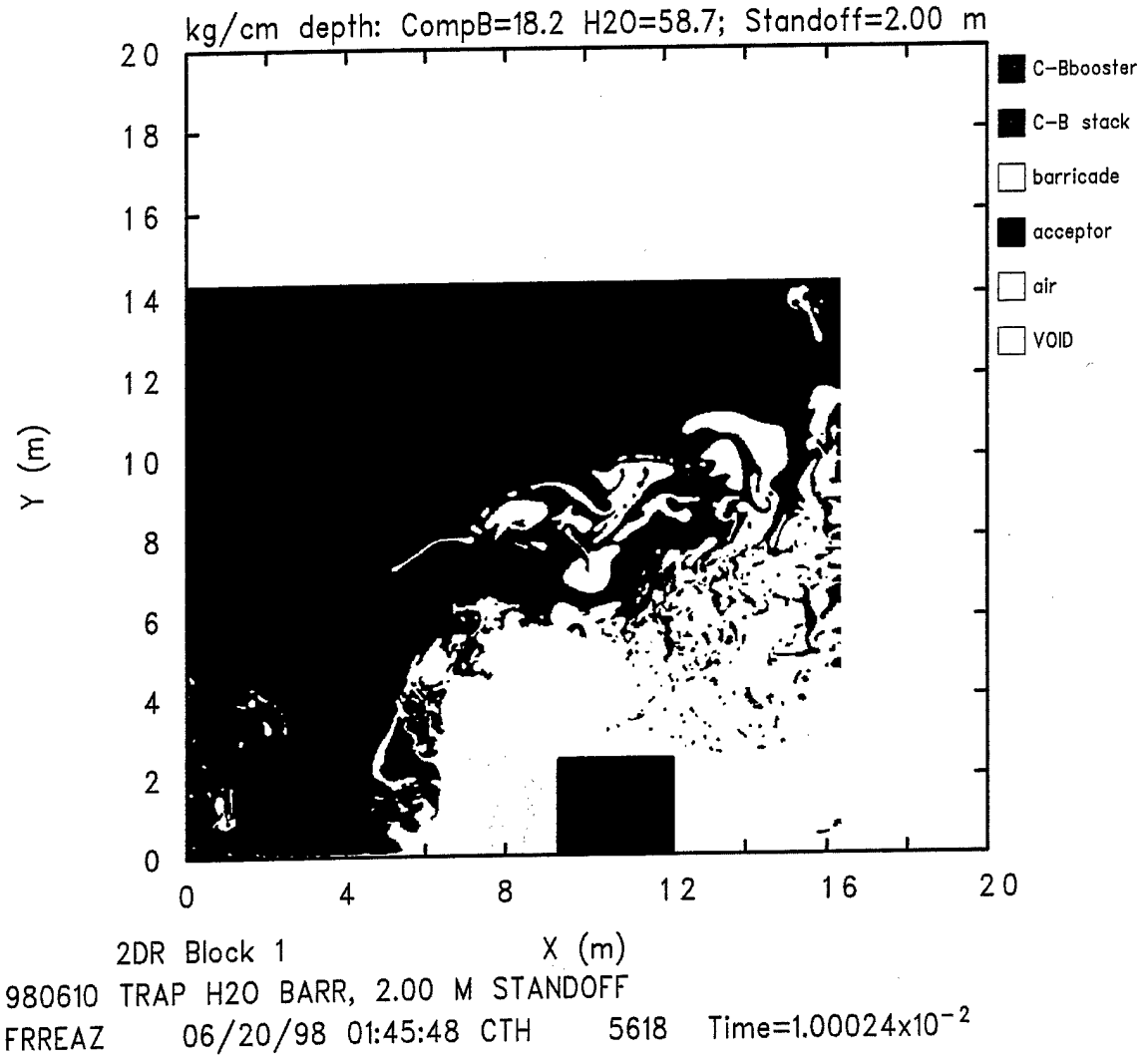

Figure 17. Flow Field at Time = 10.0 ms for Computation 980610, 2.00-m Standoff.

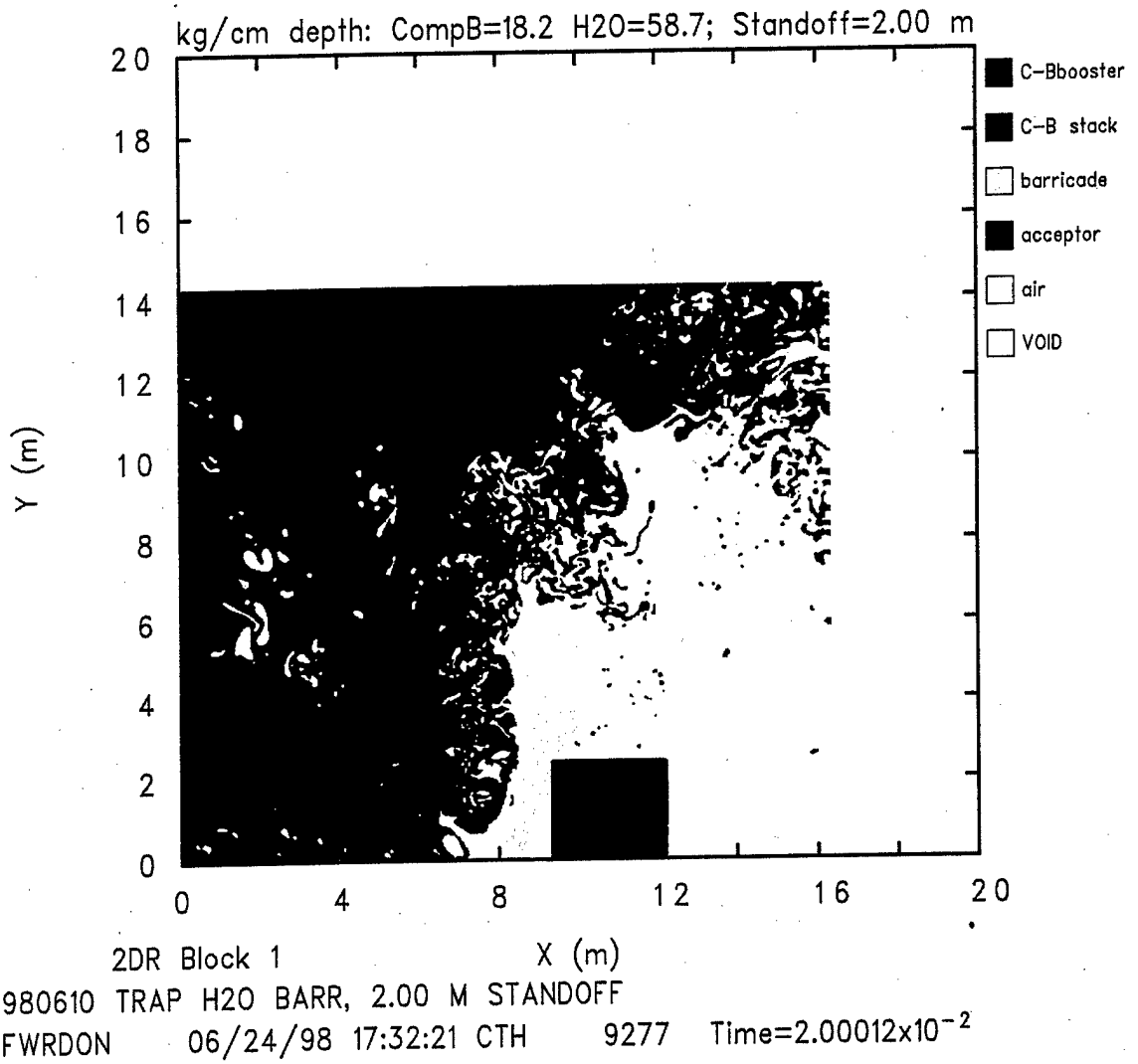

Figure 18. Flow Field at Time = 20.0 ms for Computation 980610, 2.00-m Standoff.

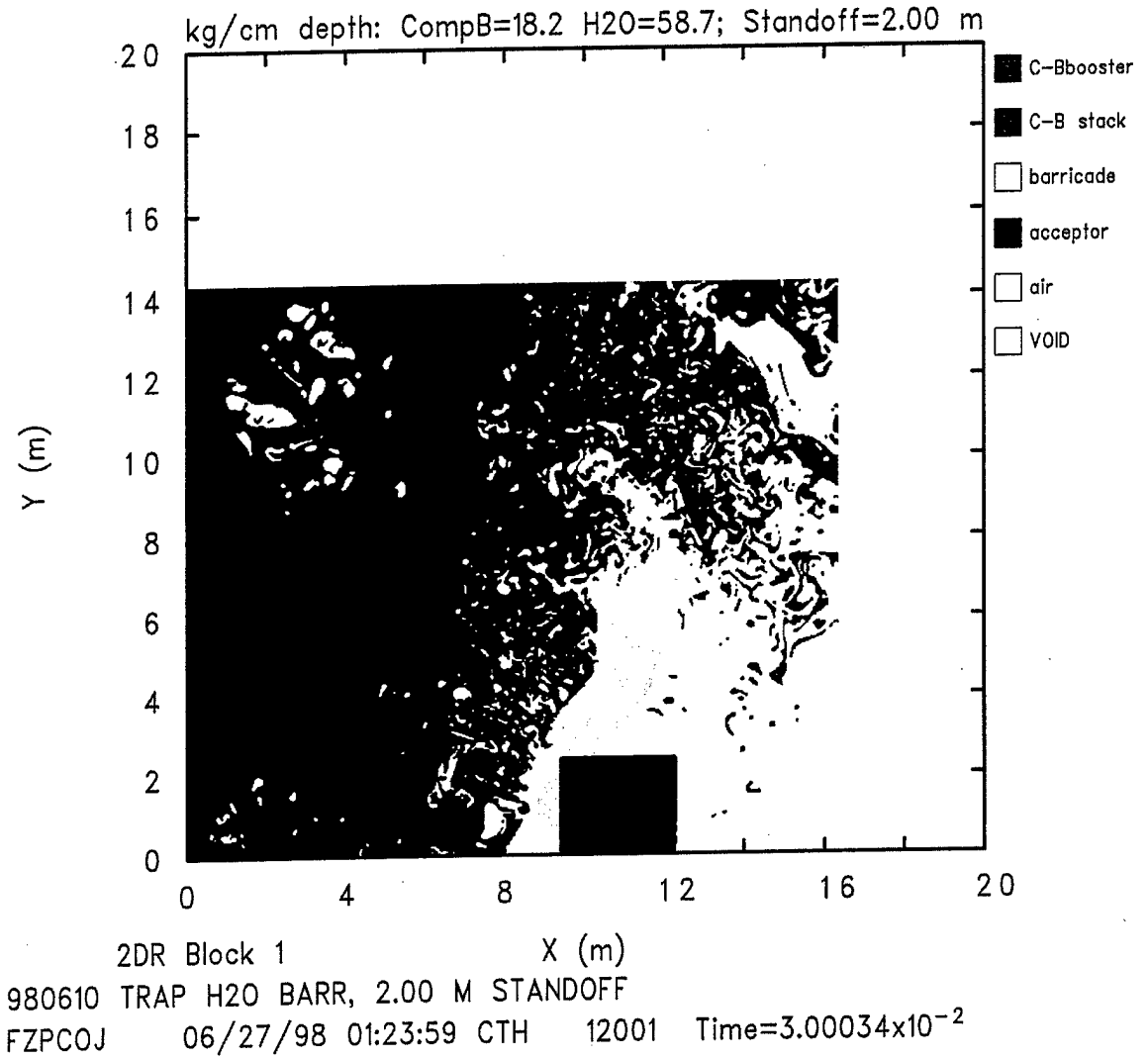

Figure 19. Flow Field at Time = 30.0 ms for Computation 980610, 2.00-m Standoff.

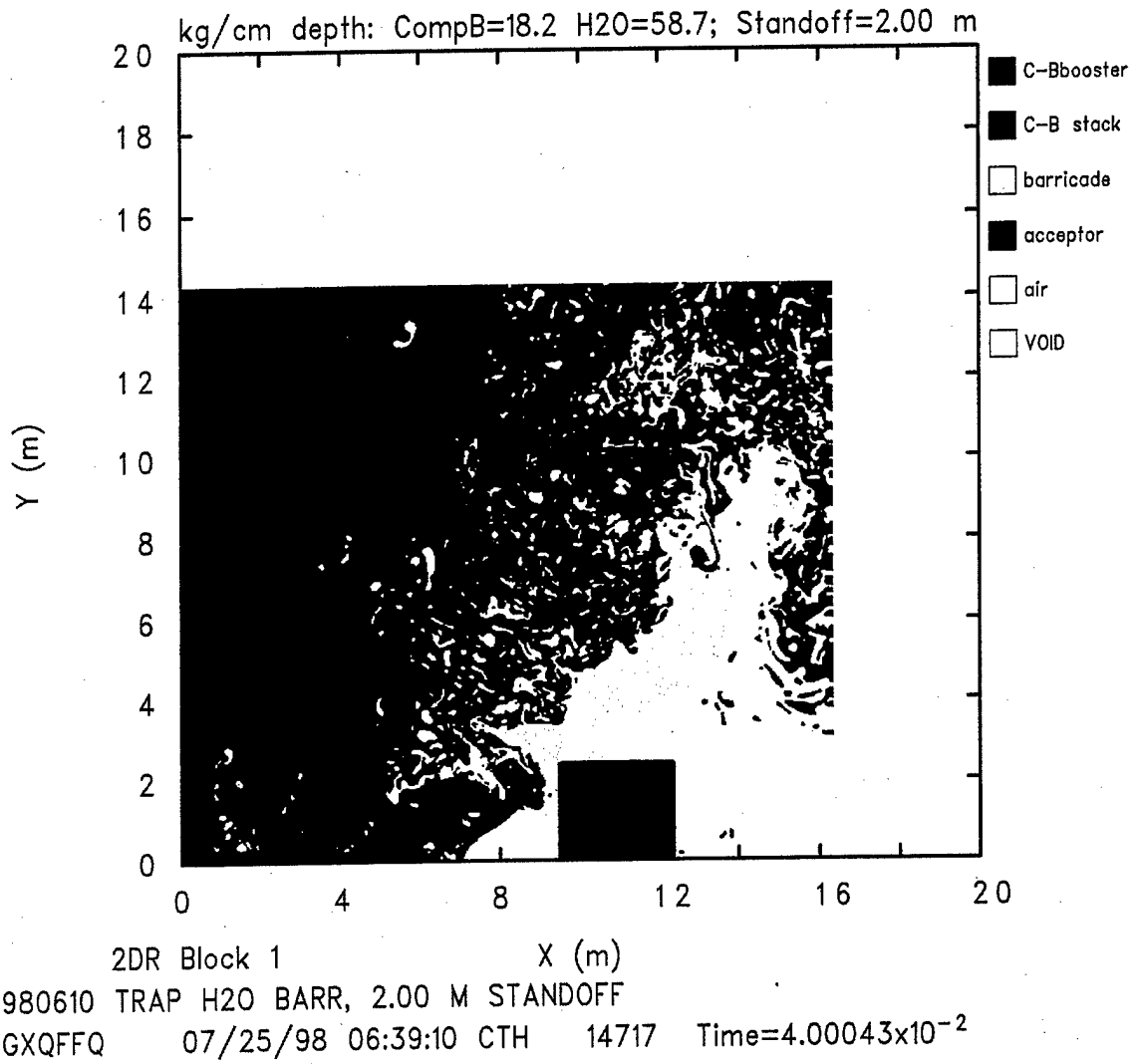

Figure 20. Flow Field at Time = 40.0 ms for Computation 980610, 2.00-m Standoff.

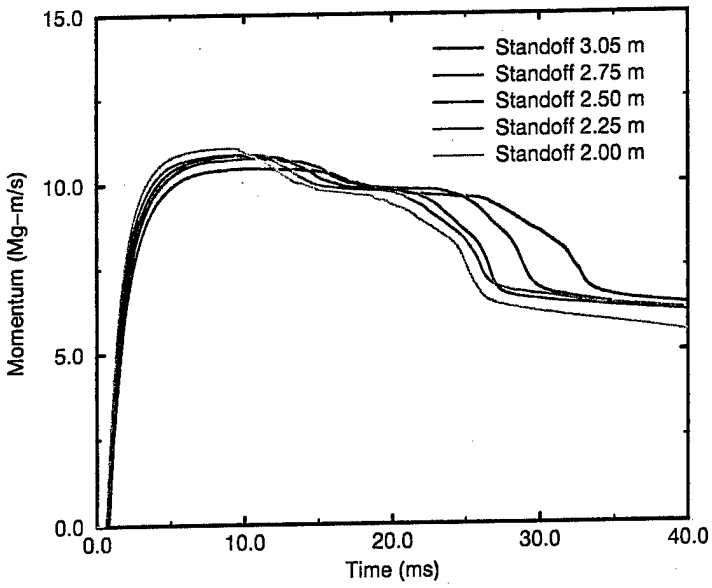

Figure 21. Water Barricade X-Direction Momentum Toward Acceptor Stack for Computations 980505 Through 980610.

the acceptor stack for each of the five fully coupled computations in this series. Hereinafter, any use of the term "momentum" or the other variables (e.g., velocity, acceleration, and displacement) derived from it should be construed as referring to the bulk value in the X direction per centimeter depth, unless specifically stated otherwise. The term "bulk" is implied but used only sparingly in order to avoid repetition. The momentum shown here is the combined momentum for all of the water in the flow field at each computational time step. Values for the mass and momentum for the water (and all other materials) are saved after each time step. During any given time step later in the computations, some water flows out of the flow field through either or both of the top and right transmissive boundaries. This accounts for at least part of the late-time trend toward decreasing momentum after 30 ms. The momentum through about 20 ms does not show a strong functional dependence upon the standoff distance. Initially, the five curves show a relatively small, monotonic increase (up to a 6 percent difference; see the following discussion) in momentum with decreasing standoff through about 10 ms. The curve for the 2.00-m standoff shows the first decrease in momentum at that time because of the impact of water from the wave on the right surface of the barricade with the top left surface of the acceptor stack. The successive drops in the curves for the greater standoff distances follow monotonically later in time with increasing standoff until they nearly converge at 20 ms. Thereafter, there is a second sequence of impacts that cause further decreases in momentum as water from the lower section on the barricade impacts the acceptor stack for each standoff. It is interesting to point out here that there is not much penalty in developing increased barricade momentum with decreased

standoff distance. The peak momentum for the 2.00-m standoff is 11.09 Mg-m/s at 8.9 ms and for the 3.05-m standoff is 10.46 Mg-m/s at 10.1 ms. This equates to a direct ratio in relative momentum of 1.060 (=11.09/10.46) for an inverse ratio in relative standoff distance of 1.524 (=3.048/2.00). Table 1 contains a summary of several X-direction parameters. The

Table 1. Barricade Peak X-Direction Bulk Motion Parameters.

Computation Number	980505	980507	980521	980528	980610
Standoff (m)	3.048	2.75	2.50	2.25	2.00
Peak Momentum (Mg-m/s)	10.46	10.76	10.85	10.89	11.09
Time (ms)	10.07	10.54	9.718	9.709	8.898
Peak Velocity (m/s)	178.2	183.4	184.8	185.5	188.8
Time (ms)	10.93	10.72	9.727	9.709	8.898
Peak Acceleration (km/s/s)	143.4	146.5	152.6	155.7	158.7
Time (ms)	10.04	9.642	8.945	8.444	8.144
Peak Left-Surface Impulse (MN-s/m)	0.9016	0.9337	0.9381	0.9502	0.9630
Time (ms)	34.48	33.42	31.03	32.46	34.22
Distance Traveled (m)	5.979	5.917	5.762	5.723	5.591
Time (ms)	39.99	39.99	39.99	39.69	39.99

parameters describe some of the bulk motion of the barricade for the various computations. First among those parameters, after the computation numbers and standoff distances, are the peak X-direction bulk momentum values for the barricade, along with their respective times of occurrence, listed with more significant figures than were typically used in the text for completeness. The rest of the parameters in the table are discussed in the following paragraphs.

The momentum curves in Figure 21 are all relatively smooth and well behaved, making it easier to extract other data from them. After each computational time step, both the total momentum and mass of the water in the flow field are known. The X-direction bulk velocity (hereinafter referred to as "X-direction velocity") of the barricade may be computed for each time step by dividing the instantaneous momentum by the corresponding mass. The X-direction velocity of the water barricade toward the acceptor stack for each standoff is shown in Figure 22. These curves are essentially scaled variants of the momentum curves shown in Figure 21 and therefore show the same relative behavior described previously. The peak X-direction velocities for the barricade at the different standoff distances are summarized in

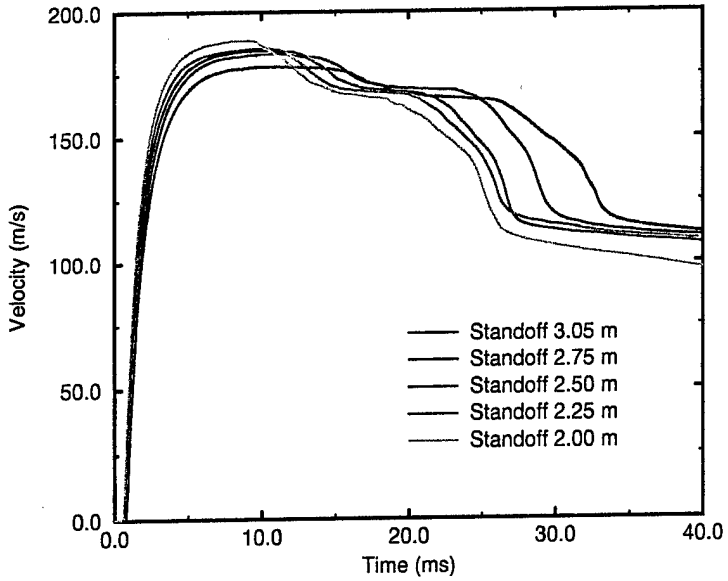

Figure 22. Water Barricade X-Direction Velocity Toward the Acceptor Stack for Computations 980505 Through 980610.

Table 1, along with their respective times of occurrence. For each standoff, the initial decrease in X-direction velocity corresponds to the impact of water from the wave on the right surface of the barricade on the top-left face of the acceptor stack. Because the computed X-direction velocity is a mass-weighted average, these initial impacts are actually occurring at higher velocities than the peaks just quoted. These initial decreases in velocity are followed by a period of nearly constant velocity, and then a second, larger decrease when the base of the barricade impacts the acceptor stack. The X-direction velocities become less meaningful at late time as far as the acceptor stack is concerned because of the increasing proportion of water that is in the air above the plane of the top face of the acceptor stack.

As noted previously, the momentum curves in Figure 21, and hence the velocity curves in Figure 22, are relatively smooth functions with respect to time. The velocities were piecewise differentiated with respect to time, using the difference values of velocity and time in the data file, to produce the curves of bulk X-direction acceleration for each standoff, as shown in Figure 23. Because the full simulation time is displayed on the abscissa, the initial accelerations of the barricade for each standoff between 0.5 and 0.9 ms appear to nearly overlay one another. The initial decelerations caused by the impact of the wave on the right surface of the barricade on the acceptor stack may be seen from about 10 through 17 ms, and the second sequence of decelerations may be seen from about 19 through 33 ms. Figure 24 shows a temporally expanded plot of the first 5 ms of the X-direction acceleration of the barricade at each standoff. The initial accelerations, all to peak values on the order

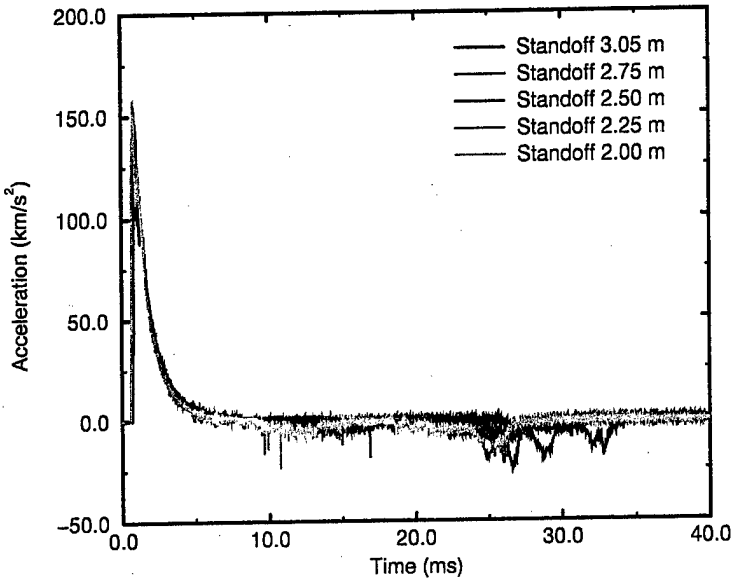

Figure 23. Water Barricade X-Direction Acceleration Toward the Acceptor Stack for Computations 980505 Through 980610.

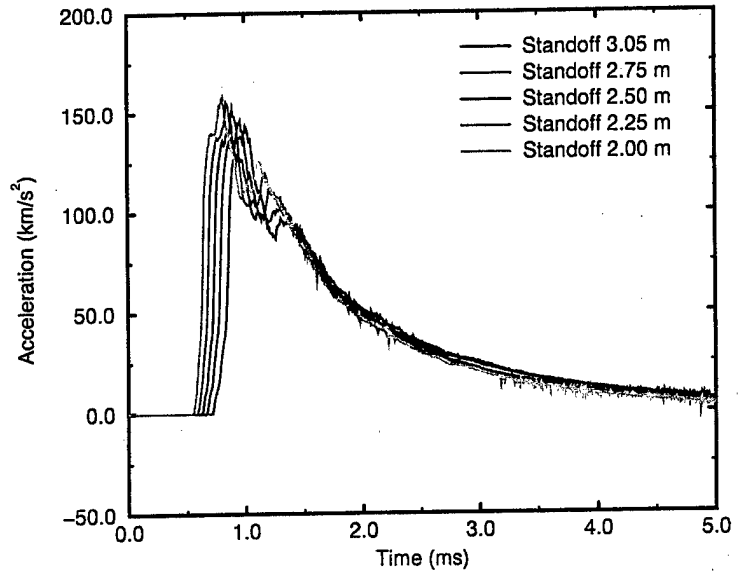

Figure 24. Water Barricade Initial X-Direction Acceleration Toward the Acceptor Stack for Computations 980505 Through 980610.

of 150 km/s^2, occur in a direct sequence based on standoff distance. Each shows a transient deceleration and reacceleration phase after about 1.0 ms caused by wave interactions that are not of primary importance to this analysis. Peak accelerations and their associated times are shown in Table 1. Most of the positive acceleration has ended by 5 ms.

The reason for this can be seen in Figure 25, which shows the X-direction total impulse per meter depth (depth is measured normal to the height-and-width plane as defined earlier) on the left surface of the barricade. This was computed by integrating the overpressure

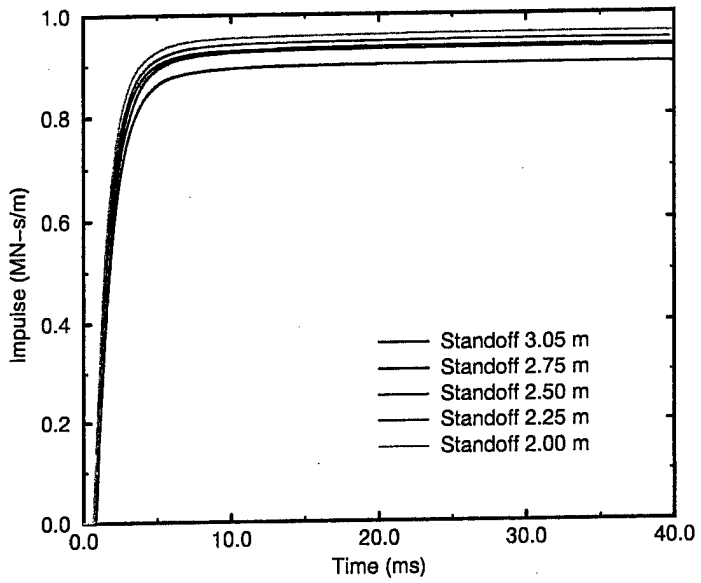

Figure 25. Water Barricade Left Surface X-Direction Total Impulse per Meter Depth for Computations 980505 Through 980610.

over space and time using 30 tracer particles that were placed along the left surface of the barricade at time zero, the grid generation time. The overpressure is the absolute pressure minus the ambient atmospheric pressure. The tracer particles were allowed to move freely with the flow in the grid. As the simulated time in the computations progressed, the left surface of the barricade became increasingly distorted. Eventually, it was no longer clearly definable as a simple surface. Correspondingly, the impulse integral itself probably lost meaning after about 10 ms. Essentially all of the impulse from the detonation of the donor stack is delivered to the barricade in the first few milliseconds. There is relatively little difference in the impulse delivered to the barricade at this range of standoff distances. The peak values and associated time are shown in Table 1. Because of the surface distortion just discussed, the times of these peaks are not particularly important and are included only for completeness. This equates to a direct ratio in relative impulse of 1.068 for an inverse ratio in relative standoff distance of 1.524.

Finally, the velocity data are used to compute the bulk translation of the barricade versus time, which is shown in Figure 26. There is relatively little differentiation in distance traveled

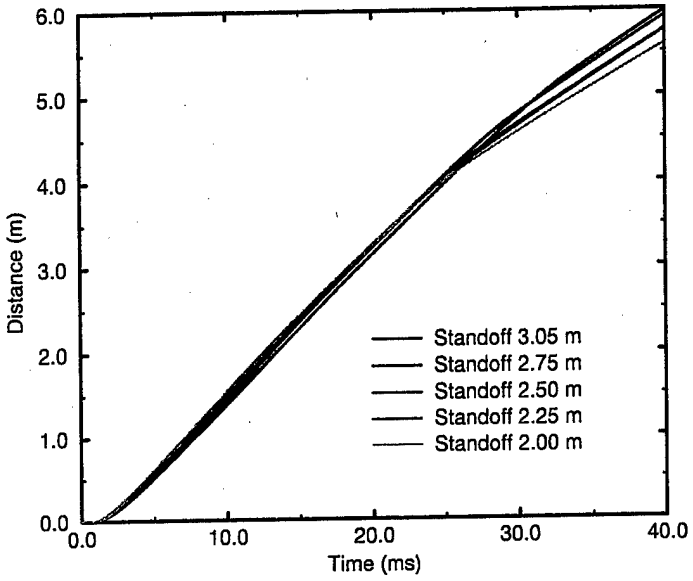

Figure 26. Water Barricade X-Direction Distance Moved Toward the Acceptor Stack for Computations 980505 Through 980610.

in relation to standoff. After about 25 ms, increasing portions of the distance traveled are by fractions of the barricade in flight above the top of the acceptor stack. The ending-time distance traveled decreases with decreasing standoff because impacts with the acceptor stack are occurring sooner (see Table 1).

Figure 27 shows the functional relations of the peak (at different times) and final (nominal 40.0 ms) values of the several parameters just described for the barricade in the preceding figures. The abscissa shows the dimensional standoff distance. The ordinate shows the normalized direct ratio of parameters, the value of a given parameter at a given standoff divided by the corresponding value for the 3.048-m standoff. Figure 28 shows the same data as shown in Figure 27, but with the abscissa showing the normalized inverse standoff ratio, computed as 3.048 m divided by each successive standoff ratio. Thus, the value for the 3.048-m standoff itself is 1.0, and the value for the 2.00-m standoff is 1.524. The ordinate is the same as for Figure 27 except for its scaling. The abscissa and ordinate scales are forced to be equal so that a $\Delta X/\Delta Y = \pm 1.0$ relationship would show as a ± 45-degree straight line. The figures show a weak functional relation of all of these normalized parameters with both dimensional and normalized standoff. This shows that, as far as these parameters for this simplified barricade are concerned, there is only a minor penalty in barricade dynamics incurred by moving the barricade closer to the donor stack to a nominal 2-m from a nominal 3-m stand-

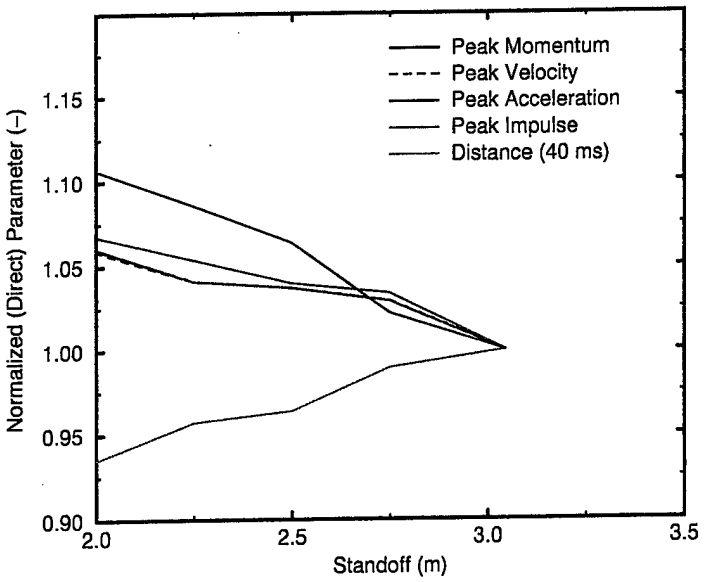

Figure 27. Normalized (Direct Ratio) Barricade Parameters Versus Standoff Distance for Computations 980505 Through 980610.

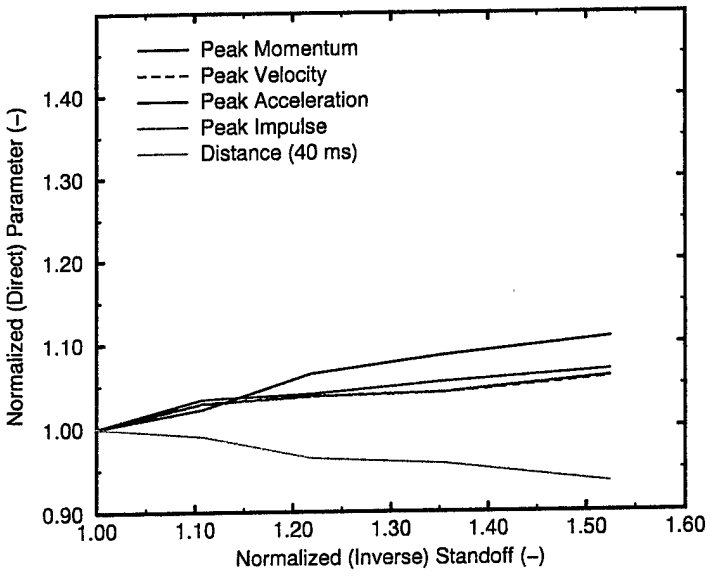

Figure 28. Normalized (Direct Ratio) Barricade Parameters Versus Normalized (Indirect Ratio) Standoff Distance for Computations 980505 Through 980610.

off. Because of their direct scaling to one another by mass, the plot for peak momentum is overlaid by the plot for peak velocity. Therefore, the peak velocity was plotted using a dashed red line. This caused what is actually a solid black line for the peak momentum to also appear on the plot as a dashed line.

3.3. Acceptor Stack Dynamics

Figure 29 shows the bulk momentum per centimeter depth of the acceptor stack in the X direction, with positive momentum defined in the positive X direction as before. The first

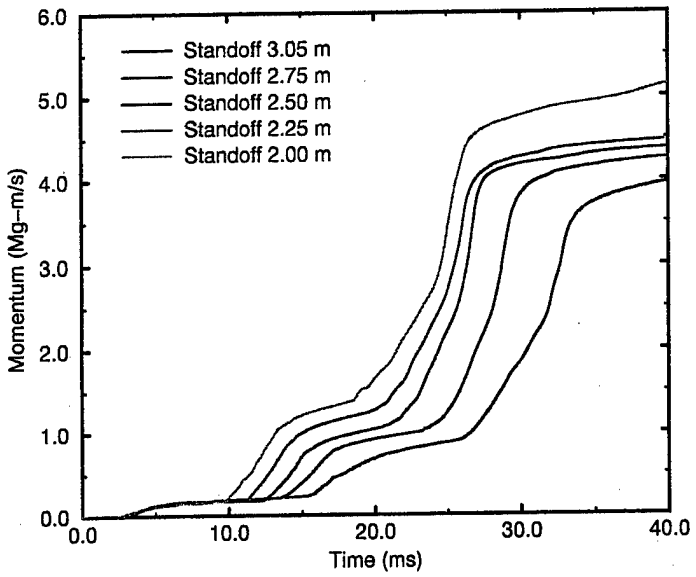

Figure 29. Acceptor Stack X-Direction Momentum for Computations 980505 Through 980610.

increase in momentum of the acceptor stack for the various standoffs that occurs from 2.5 ms through 10 ms is caused by the loading of the air shock on the acceptor stack left face. This air shock has been considerably weakened by the process of diffracting over the barricade. It is a relatively minor contributor to the overall momentum. The second set of increases in momentum can be seen starting at 10 ms, with the first in that set for the 2.00-m standoff at 10 ms and the last at somewhat less than 16 ms for the 3.05-m standoff. These increases in acceptor stack momentum are caused by the impact of water from the wave on the right surface of the barricade on the top of the left face of the acceptor stack. The third set of increases is caused by the impact of the bottom section of the barricade on the acceptor stack. The first of that set begins at about 18 ms for the 2.00-m standoff, and the last at about 26 ms for the 3.05-m standoff. The final values at 40.0 ms range from 3.96 Mg-m/s for

the 3.05-m standoff to 5.14 Mg-m/s for the 2.00-m standoff, with all curves still showing a moderate positive slope. Table 2 contains a summary of several X-direction parameters that describe some of the bulk motion of the acceptor stack for the various computations. First among those parameters, after the computation numbers and standoff distances, are the peak X-direction bulk momentum values for the acceptor stack, along with their respective times of occurrence, listed with more significant figures than were typically used in the text for completeness. The rest of the parameters in the table are discussed in the following paragraphs.

Table 2. Acceptor Stack Peak X-Direction Bulk Motion Parameters.

Computation Number	980505	980507	980521	980528	980610
Standoff (m)	3.048	2.75	2.50	2.25	2.00
Peak Momentum (Mg-m/s)	3.962	4.259	4.376	4.469	5.141
Time (ms)	40.00	40.00	40.00	39.70	40.00
Peak Velocity (m/s)	33.40	35.91	36.90	37.68	43.34
Time (ms)	40.00	40.00	40.00	39.70	40.00
Peak Acceleration (km/s/s)	9.277	10.33	11.89	10.88	10.33
Time (ms)	32.80	28.66	26.67	26.04	24.87
Peak Left-Surface Impulse (kN-s/m)	372.5	404.4	419.5	427.9	494.5
Time (ms)	39.99	39.99	39.99	39.69	39.99
Distance Traveled (cm)	40.65	54.07	63.34	67.87	80.19
Time (ms)	39.99	39.99	39.99	39.69	39.99

The corrected mass of the acceptor stack was used to compute the bulk X-direction velocity from the momentum of the acceptor stack. The results are shown in Figure 30. The curves show the same timing and differentiation as those for the acceptor stack momentum. The velocities at 40.0 ms range from 33.4 m/s (3.05-m standoff) to 43.3 m/s (2.00-m standoff) (see Table 2).

As was done for the barricade, the acceptor stack velocity for each standoff was piece-wise differentiated with respect to time to compute the bulk X-direction acceleration of the acceptor stack. The acceleration curves are shown in Figure 31. Each individual curve shows a clear three-stage acceleration sequence as time progresses. The first acceleration for each standoff occurs at about 2.5 ms, with each acceleration less than 1.0 km/s^2. These are

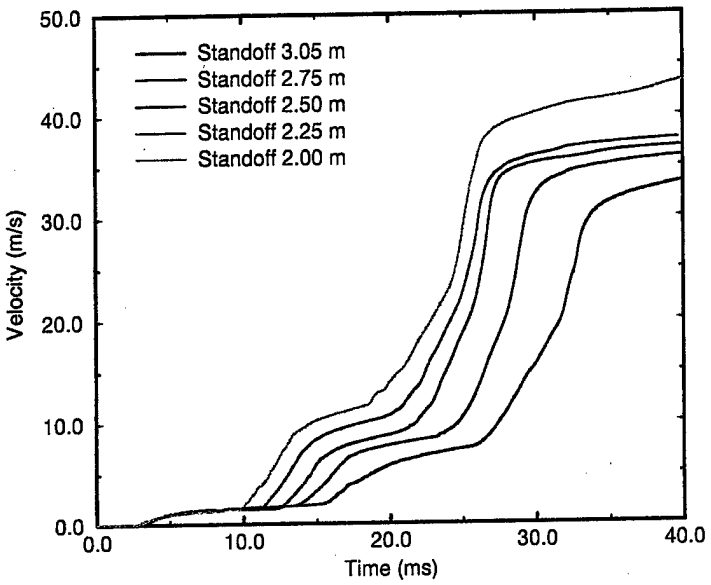

Figure 30. Acceptor Stack X-Direction Velocity, Computations 980505 Through 980610.

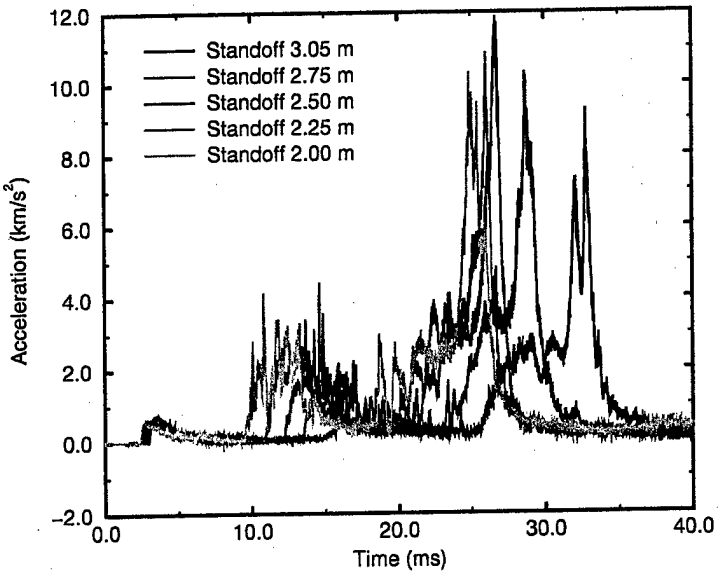

Figure 31. Acceptor Stack X-Direction Acceleration for Computations 980505 Through 980610.

caused by the diffracted air shock. The second acceleration sequence, from approximately 10 to 16 ms, is caused by the impact of water from the wave on the right surface of the barricade and ranges from 2.0 to 4.5 km/s^2. The third acceleration sequence, from approximately 18 to 26 ms with peaks from about 9 to 12 km/s^2, is caused by the impact of the lower section of the barricade on the acceptor stack, with the peak for the 2.50-m standoff probably a geometric effect caused in part by the 2-D Cartesian simplifications employed here (see Table 2).

The acceptor stack was modeled as a solid iron rectangle so that the most reliable loading possible could be computed for its left face. Thirty tracer particles were uniformly spaced along the left face, top to bottom, of the acceptor stack. They were constrained from moving in either the X or Y direction so that the ensuing hydrodynamic flows would not sweep them off the face of the acceptor stack or reposition them horizontally or vertically. Modeling the acceptor stack as a solid iron mass in the computation resulted in having relatively little movement of the acceptor stack relative to the fixed tracers on its left face during the time of the main loading. Fixing the tracer particles in space allowed a reliable overpressure integration. The overpressure histories were integrated over space and time to compute the total X-impulse per meter depth versus time for each standoff. These curves are shown in Figure 32. The acceptor stack shows a somewhat greater effect of standoff on the total impulse delivered to it than does the left surface of the barricade. The peak values are shown in Table 2.

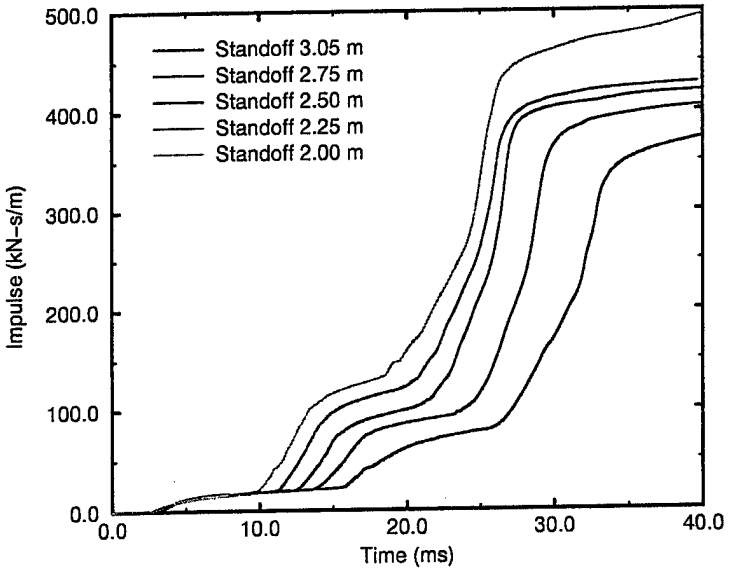

Figure 32. Acceptor Stack X-Direction Total Impulse per Meter Depth for Computations 980505 Through 980610.

Figure 33 shows the distance that the acceptor stack moves as a result of the blast and impact loading by 40.0 ms. The distance computation used the acceptor stack velocity based on the correct acceptor stack mass. The distances computed using the correct acceptor stack mass are much greater than the apparent movement of the massive acceptor stack that might be inferred from the earlier flow field plots. The range of X-direction movement for the acceptor stack is from 40.6 cm (3.05-m standoff) to 80.2 cm (2.00-m standoff) (see Table 2).

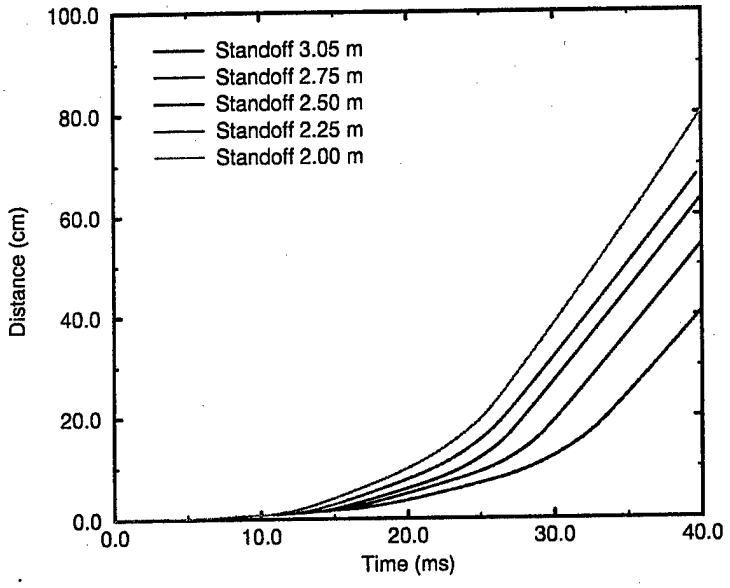

Figure 33. Acceptor Stack X-Direction Distance Moved for Computations 980505 Through 980610.

Figure 34 shows the functional relations of the peak (at different times) and final (at 40.0 ms) values of the several parameters versus standoff that were just described for the acceptor stack in the preceding figures. The ordinate parameters are normalized in the same way as was done in Figure 27. They are computed as the direct ratio of the respective parameters relative to the values for the 3.05-m standoff. Figure 35 shows the same ordinate data (rescaled) plotted against the inverse normalized standoff, with that normalization done in the same way as for Figure 28 and with equal scaling of the data forced for both axes. Figure 35 shows stronger correspondences than for the barricade for the normalized peak momentum and peak velocity (with the dashed red line for the velocity overlaid once again so that the solid black line for the momentum also appears to be a dashed line), and the peak impulse curves, but still not an overall one-to-one ratio. The peak acceleration curve shows a one-to-one correspondence through a normalized inverse standoff ratio of 1.22 (standoff from 3.05 m through 2.50 m), but falls off rapidly thereafter. This may be a geometric effect caused by the simplified 2-D Cartesian representation of the layout of the donor stack,

barricade, and acceptor stack. The distance traveled by 40.0 ms shows a greater than one-to-one correspondence with normalized inverse standoff. Additionally, the relationship of distance traveled by the acceptor stack with normalized inverse standoff is opposite that of the distance traveled by the barricade with normalized inverse standoff (see Figure 28).

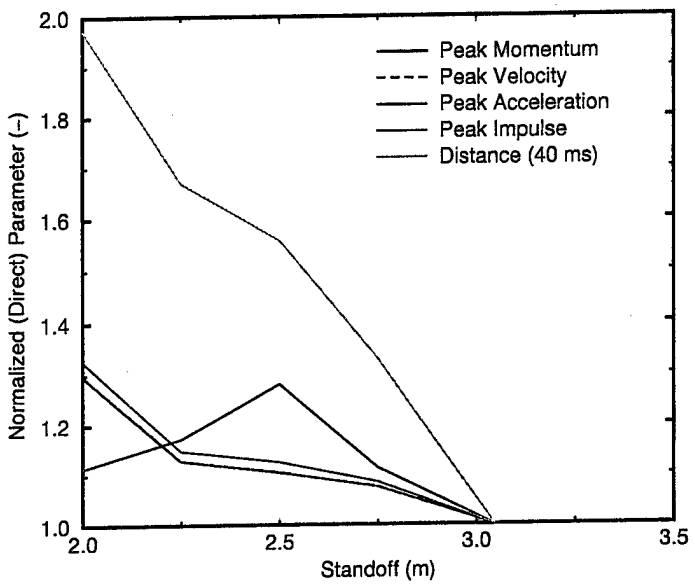

Figure 34. Normalized (Direct Ratio) Acceptor Stack Parameters Versus Standoff Distance for Computations 980505 Through 980610.

The simple standoff distance, measured from the stack base to the barricade base, may not be the only meaningful distance to consider when examining these parameters for the acceptor stack. The total distance between the right face of the donor stack and the left face of the acceptor stack, equal to twice the standoff plus the base width of the barricade, may be an informative parameter to use. For convenience, this distance is hereinafter referred to as "face separation." Figure 36 shows the ordinate values from Figures 34 and 35 plotted against an abscissa showing the face separation. Figure 37 shows the same ordinate data plotted against the inverse normalized face separation. The normalizing value in the numerator was the face separation for the 3.05-m standoff. One-to-one scaling for the normalized abscissa and ordinate was forced in this figure. The normalized peak momentum, velocity, and impulse show a nearly one-to-one correlation with the inverse normalized face separation. The peak acceleration shows a strong peak at the middle standoff of 2.50 m, and the normalized distance shows almost a five-to-one relation. There are certainly more parameters to be considered in determining functional relations such as these. Among the more important are barricade shape, mass, and material composition; explosive charge mass;

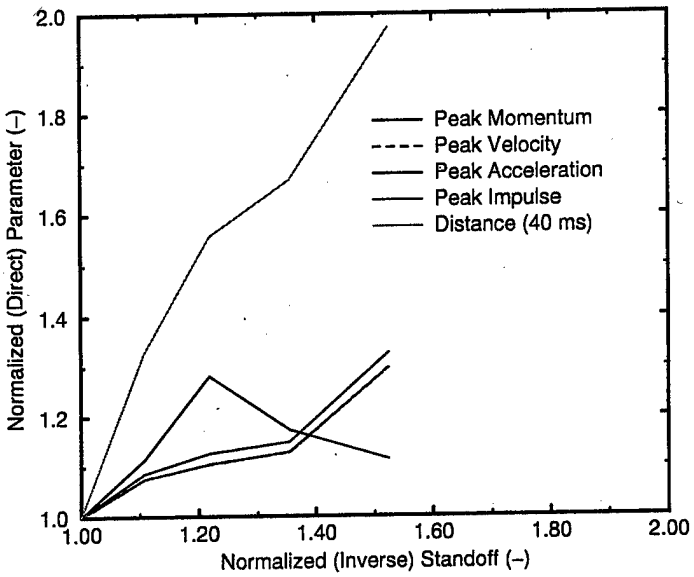

Figure 35. Normalized (Direct Ratio) Acceptor Stack Parameters Versus Normalized (Inverse Ratio) Standoff Distance for Computations 980505 Through 980610.

and 3-D considerations. These factors will be explored to the extent possible within the time and funding constraints of this project.

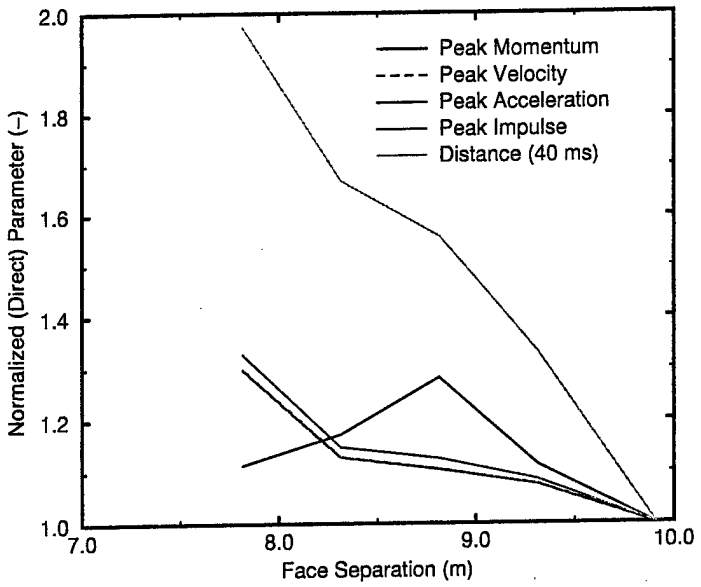

Figure 36. Normalized (Direct Ratio) Acceptor Stack Parameters Versus Face Separation for Computations 980505 Through 980610.

3.4. Acceptor Stack Left Surface Pressures

The pressures on the surface of the acceptor stack during this type of event are of great interest. Data from the 30 tracers that were placed uniformly along the left surface of the acceptor stack were processed to present a comprehensive summary of the overpressure history on that surface for each computation. An area-weighted average overpressure was computed using all of the 30 individual tracer pressures at each point in time. The maximum overpressure for any of the tracers at a given time was identified, as was the minimum. Figure 38 shows the overpressure on the left surface of the acceptor stack for a standoff of 3.05 m. The diffracted air shock loading that occurs from about 3 to 6 ms is relatively small in both average and peak values. The negligible loading between 6 and 15 ms occurs because the air blast has already passed by and the barricade is the process of distorting and translating toward the acceptor stack, but no sections have yet arrived. The loading from 15 to 25 ms is primarily from the impact of water from the wave on the right surface of the barricade on the top-left surface of the acceptor stack. The average overpressures during that period are well below 25 MPa, but some peak values are at 100 MPa (1.0 kbar) or greater. (A cautionary note is in order here. Individual, temporally narrow pressure peaks in or

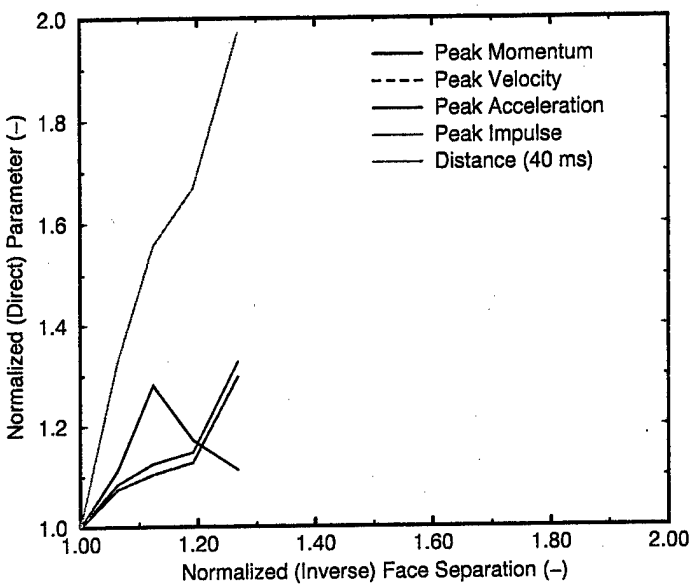

Figure 37. Normalized (Direct Ratio) Acceptor Stack Parameters Versus Normalized (Inverse Ratio) Face Separation for Computations 980505 Through 980610.

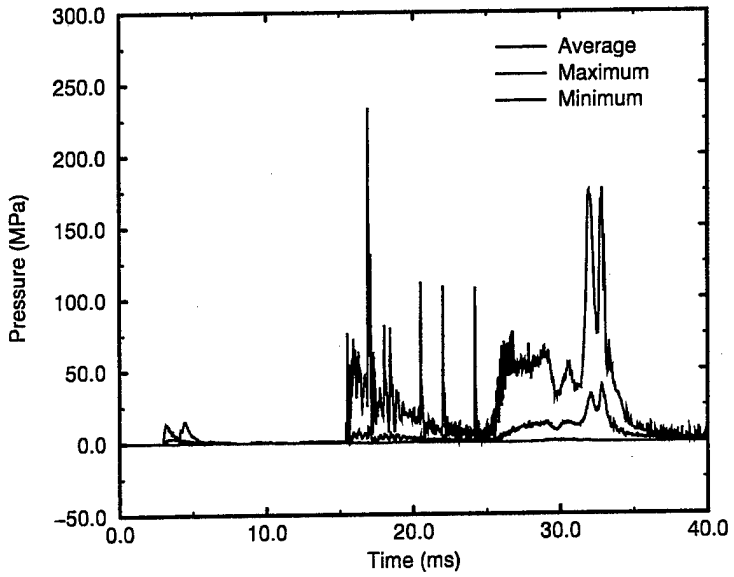

Figure 38. Acceptor Stack Left Surface Overpressure, 3.05-m Standoff, Computation 980505.

near mixed-material cells in an explicit time-stepping Eulerian hydrocode should be viewed with caution. While they may very well be valid, they should not necessarily be accepted as numerically accurate without corroborating indicators from other thermodynamic state and mechanical material properties.) The main loading phase occurs between 25 and 36 ms. This is when the majority of the impulse is delivered to the left surface of the acceptor stack. Figure 38 is particularly useful in helping to better understand the shape of the impulse curve for the 3.05-m standoff shown in Figure 32. The same distinct three-phase loading sequence for the left surface of the acceptor stack can be seen in Figure 39 for the 2.75-m standoff,

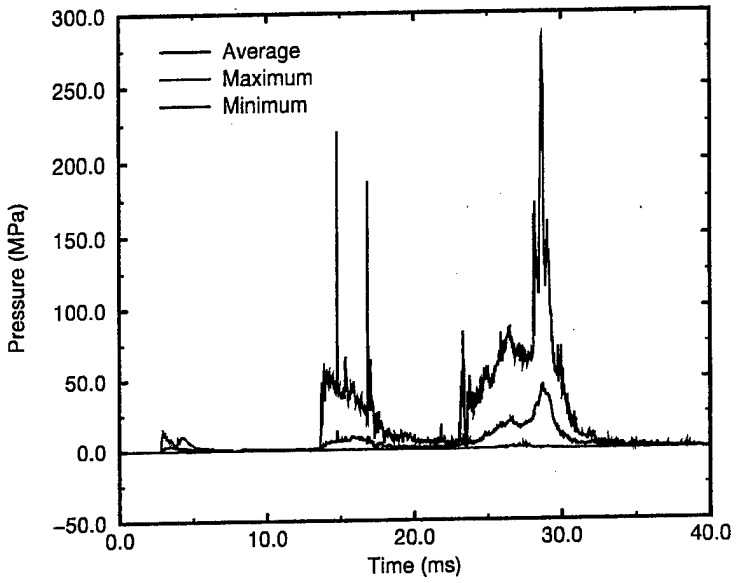

Figure 39. Acceptor Stack Left Surface Overpressure, 2.75-m Standoff, Computation 980507.

Figure 40 for the 2.50-m standoff, Figure 41 for the 2.25-m standoff, and Figure 42 for the 2.00-m standoff. No overpressure peaks above 300 MPa (3 kbar) were computed on the left surface of the acceptor stack for any of the fully coupled computations. An excellent summary report by Liddiard and Forbes[18] stated, for example, that the underwater sensitivity test (UST) showed that "...compression by a 3 or 4 kbar shock is, of itself, a sufficient external stimulus to start chemical reaction in a heterogeneous solid explosive such as pentolite..." and "...UST burning occurs at peak stresses of 4 to 12 kbar in the explosives..." Thus, the pressure peaks computed here on the outside surface of the acceptor stack are just below the minimum values reported to be capable of starting a chemical reaction. It should be stressed here that these are computed peaks on a simplified flat iron surface using a modest computational grid resolution of 4.0 cm. A transmitted peak through an iron shell and into an explosive fill in a simplified geometry would likely be smaller because of impedance mismatches at the surfaces, but finer gridding would likely produce greater peaks. Surface curvatures typical of munitions would reduce peak surface and transmitted pressures, but

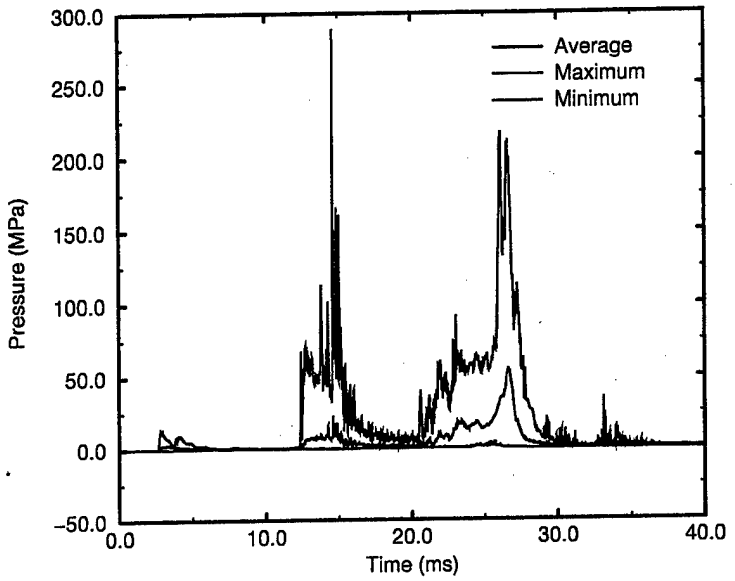

Figure 40. Acceptor Stack Left Surface Overpressure, 2.50-m Standoff, Computation 980521.

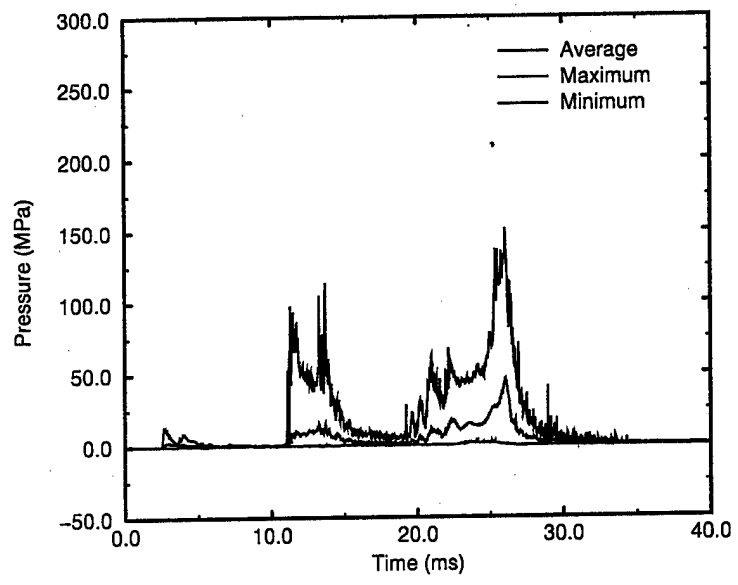

Figure 41. Acceptor Stack Left Surface Overpressure, 2.25-m Standoff, Computation 980528.

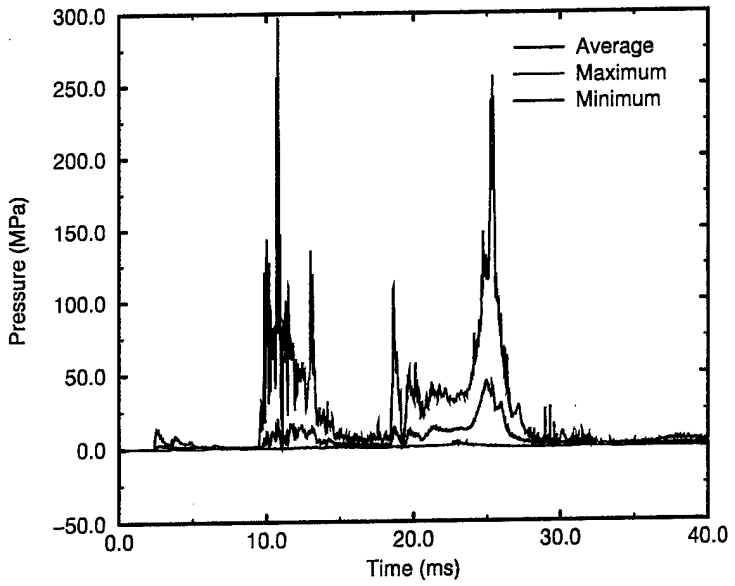

Figure 42. Acceptor Stack Left Surface Overpressure, 2.00-m Standoff, Computation 980610.

secondary impacts of accelerated individual munitions against one another could produce greater peaks.

3.5. Coupled Versus Uncoupled Acceptor Stack Dynamics at 3.05-m Standoff

A previous report[1] presented the results of an uncoupled pair of computations for the same donor and acceptor munitions stacks and trapezoidal water barricade at a standoff of 3.05 m. It is now instructive to compare the dynamics of the acceptor stack as computed in the uncoupled pair of computations to the fully coupled Computation 980505. When necessary, the abscissa-and-ordinate scalings of plots are forced to be the same as those in the previous section in order to make visual comparisons between figures easier, even if the stand-alone scaling of some of the figures to follow appears to be somewhat unusual.

The dynamics of the barricade in the first 8.00 ms of Computation 980505 and through the total 8.00 ms simulated time in Computation 970908 were essentially the same as one another (different versions of CTH were used), so a comparison of barricade responses is not made. The same is true for the blast loading through 8.00 ms on the acceptor stack left face computed in 970908. Based upon simplified estimates of the barricade location together with the X-direction velocity at the end of Computation 970908, it was estimated[1] that the arrival time of the barricade at the left face of the acceptor stack would be about 19.7 ms after initiation. Figure 43 shows the X-direction momentum for the acceptor stack

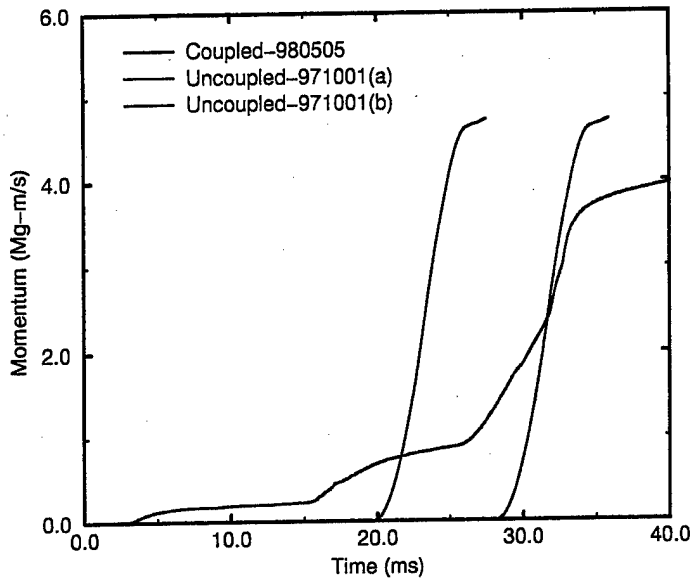

Figure 43. Acceptor Stack X-Direction Momentum, Coupled Versus Uncoupled Computations, 3.05-m Standoff.

for Computation 980505, plus two time-shifted variants of the acceptor stack momentum from Computation 971001 having identical ordinate values to those previously reported.[1] The first of those two time-shifted variants, labeled "Uncoupled-971001(a)," has a positive time shift of 19.7 ms in accordance with that previous estimate. This shows the acceptor stack gaining its momentum at a much faster rate and starting to do so at an earlier time than the fully coupled computation. An additional time shift of 8.42 ms was then added to move the uncoupled momentum curve farther out in time to force the intersection of that new curve, labeled "Uncoupled-971001(b)," to be at a nearly mid-range inflection point in the coupled momentum curve. This seemed to provide a reasonable synchronization of the curves for the two computations, so the second time shift which totaled 28.12 ms is the only one used for the remaining comparisons. The final value for the momentum for the uncoupled computation is 4.74 Mg-m/s compared with 3.96 Mg-m/s for the fully coupled computation, greater by 19.7 percent.

Figure 44 shows a comparison of the acceptor stack velocity for the coupled versus uncoupled (28.12 ms time shift) computations. As expected, the relative shapes are the same as for the momentum curves because of the simple scaling by the acceptor stack mass. The final velocity for the uncoupled computation is 40.0 m/s versus 33.4 m/s for the coupled computation, with the uncoupled velocity still rising at a faster rate than that for the coupled computation.

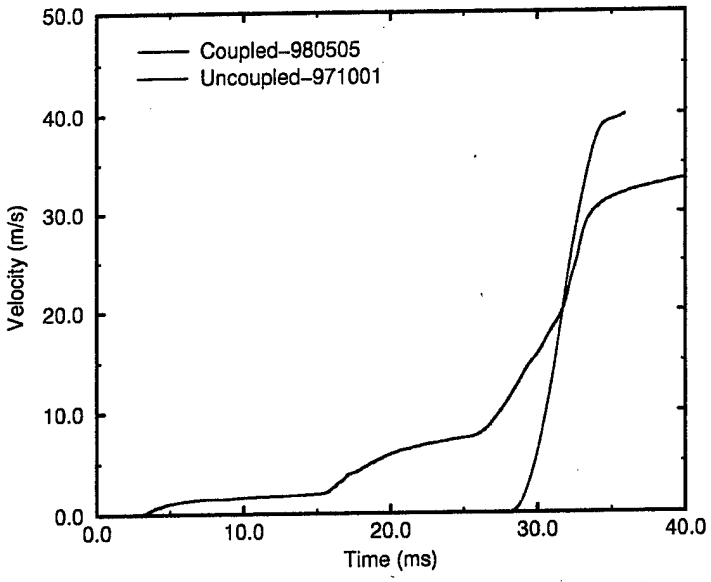

Figure 44. Acceptor Stack X-Direction Velocity, Coupled Versus Uncoupled Computations, 3.05-m Standoff.

Figure 45 shows a comparison of the acceptor stack X acceleration for the coupled versus uncoupled computations. While the peak acceleration of 10.3 km/s^2 for the uncoupled computation is only 11.0 percent greater than the 9.28-km/s^2 peak for the coupled computation, there are significant differences. The uncoupled computation has a much narrower overall acceleration curve compared with the three-stage acceleration shown in the coupled curve, but it is much broader than the third and greatest acceleration phase in the coupled computation. The respective curves for impulse per meter depth are shown in Figure 46. They show the same relative behavior as for the acceleration curves. The X-direction impulse at the end of Computation 971001 is 468.3 kN-s/m, which is 25.7 percent above the 372.5 kN-s/m at the ending of 980505, with that for 971001 still rising at a faster rate.

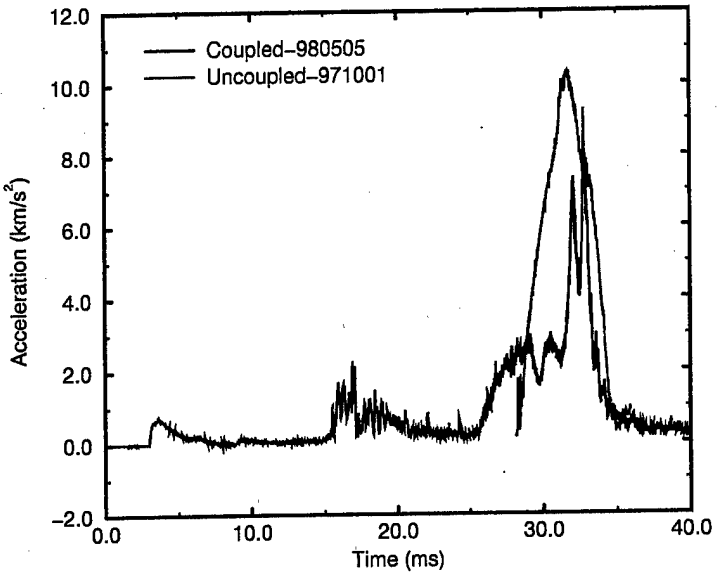

Figure 45. Acceptor Stack X-Direction Acceleration, Coupled Versus Uncoupled Computations, 3.05-m Standoff.

Figure 47 shows a comparison of the computed values of the distance that the acceptor stack moves as a whole body. This is another good indicator of the value of performing fully coupled computations whenever possible and practical. Even though the ending-time velocity and impulse and the peak acceleration in the uncoupled computation are all greater than the respective values from the coupled computation, the distance traveled during the simulated 7.80 ms time in Computation 971001 is less (17.0 cm) at its shifted ending time of 35.9 ms than the corresponding 27.3 cm for the coupled computation at that same time. If the 1.58 m/s ending-time (at 8.0 ms) velocity of the acceptor stack in Computation 970908 is factored in by adding a distance traveled at an average of one-half of 1.58 m/s for the first 8.0 ms, plus a distance traveled at 1.58 m/s for the next 20.12 ms (28.12 ms minus 8.00 ms),

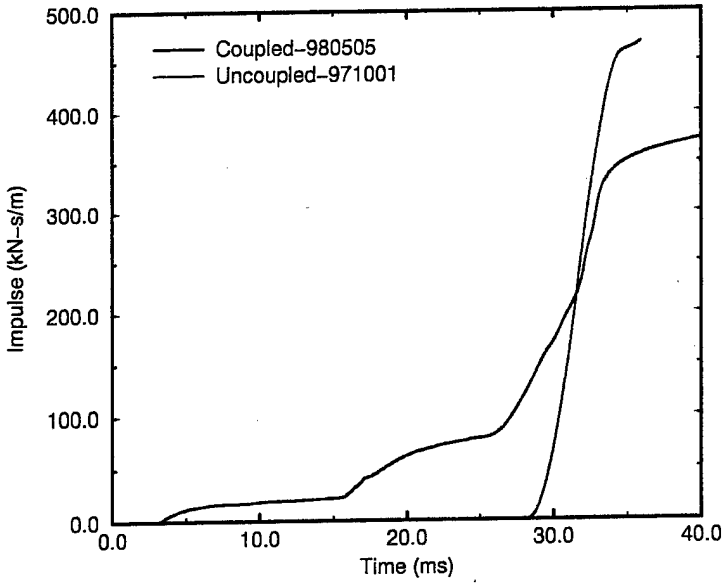

Figure 46. Acceptor Stack X-Direction Total Impulse per Meter Depth, Coupled Versus Uncoupled Computations, 3.05-m Standoff.

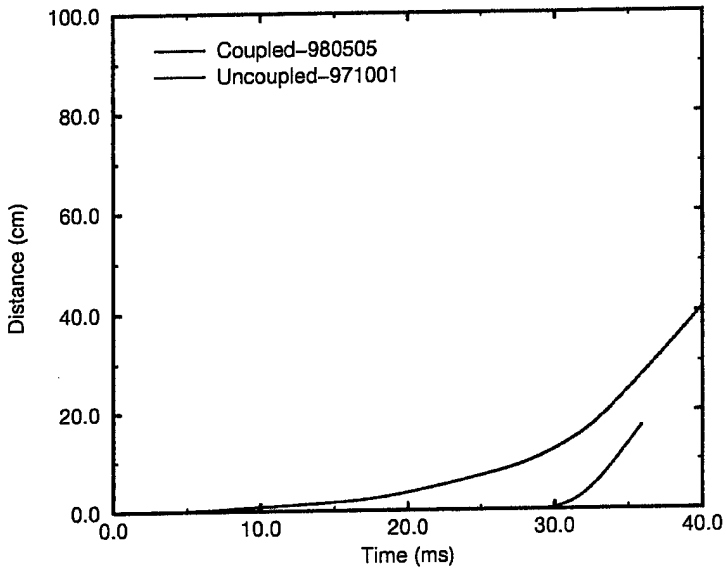

Figure 47. Acceptor Stack X-Direction Distance Moved, Coupled Versus Uncoupled Computations, 3.05-m Standoff.

then the uncoupled distance curve would be shifted upward by 3.81 cm to a value of 20.8 cm at 35.9 ms. Because the X-direction velocity in 971001 at 35.9 ms is greater than even the velocity in 980505 at 40.0 ms, Computation 971001 predicts a greater ultimate distance moved in the absence of surface forces such as friction and body forces such as additional impacts.

Figure 48 is simply Figure 38 with the ordinate rescaled for convenience in comparing with Figure 49, which shows the time-shifted overpressure on the left surface of the acceptor stack for the uncoupled Computation 971001. The peak overpressure in 971001 is 487 MPa (4.87 kbar), and the greatest average overpressure in 971001 is 50.0 MPa (0.500 kbar). This compares with a peak overpressure of 234 MPa (2.34 kbar) and maximum average overpressure of 38.9 MPa (0.389 kbar) for computation 980505. The pressure peak shown in Computation 971001 is above the minimum value reported by Liddiard and Forbes[18] as capable of starting a chemical reaction if it were experienced by the explosive fill of one of the munitions in a similar test. The comparisons in this section demonstrate that the previously reported[1] results from the two uncoupled computations represented a worst case for this simplified 2-D Cartesian simulation.

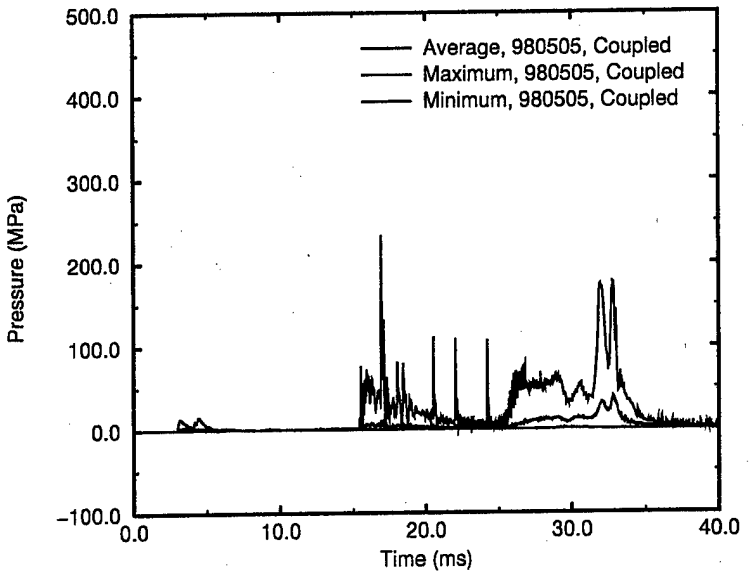

Figure 48. Acceptor Stack Left Surface Overpressure, 3.05-m Standoff, Coupled Computation 980505 (Rescaled).

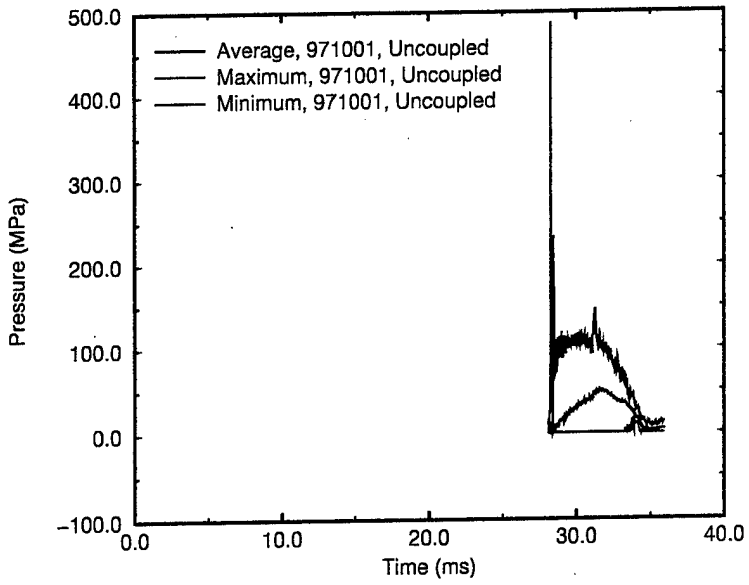

Figure 49. Acceptor Stack Left Surface Overpressure, 3.05-m Standoff, Uncoupled Computation 971001.

4. CONCLUSION

The coupled computations discussed herein modeled a simplified, uncased, rectangular explosive charge representing a nominal munitions stack containing 4,000 kg of Comp-B undergoing a complete, high-order detonation with the initiation point at its center. No munitions casings or packing materials (and their resulting fragments) were included. The only barricade design that was used was a solid, water-only trapezoid with sides having a 30-degree angle to the vertical. A geometrically simplified 2-D Cartesian coordinates system with the same finite-difference grid was used throughout the computations. This eliminated 3-D divergence effects that could reduce loadings considerably. The only parameter that was varied was the standoff distance.

These computations demonstrate a relatively weak inverse functional relationship between normalized values of the standoff distance and the loading on and whole-body response of the barricade. A moderate inverse functional relation was found between the normalized values of standoff distance and the responses of the acceptor stack, and a stronger relation was found when munitions stack face separation was used. The sloping sides of the barricade, together with its relatively large mass, were effective in deflecting much of the blast upward and away from the acceptor stack. None of the five computations showed any contact by the explosive products with the acceptor stack through the 40.0 ms simulated time, although the possibility of contact after this time can be inferred by analyzing the changing

configurations of the materials shown in the late-time flow field plots. For a simple, single high-order detonation event *without fragment generation (which is not a realistic situation)*, this study indicates that there may not be a great penalty in having a massive barricade with sloping sides at, for example, a 2-m versus 3-m nominal standoff distance. The loading on the acceptor stack for all computations was a three-stage process: (1) a weak air shock, (2) an impact of water from the wave on the right surface of the barricade on the top of the left surface of the acceptor stack, and (3) the greatest loading from the impact of water from the lower section of the barricade on the middle and bottom of the left face of the acceptor stack. The acceleration of and impulse on the acceptor stack was also a three-stage process for the same reasons. The peak pressures on the left surface of the acceptor stack were marginally below published minimum stress levels that are capable of causing chemical reactions in heterogeneous explosives.

A comparison was made between a fully coupled computation for a standoff distance of 3.05 m with a previously reported uncoupled pair of loading and impact computations for the same standoff by the author. This comparison showed that the uncoupled computations provided a worst-case estimate of the loading on and whole-body response of the acceptor stack. However, the differences were great enough to show the value of performing fully coupled computations whenever possible and practical.

A significant missing element in the computational series reported here is a determination of the synergistic effects of the impact of large numbers of high-speed fragments along with the relatively extreme air blast and explosive products impact loading that a barricade would experience in the detonation of an actual munitions stack. A simple high-order detonation of all of the energetic material within a munitions stack with no fragment and debris generation is probably the most benign event possible against which to a design a barricade. In that event, a barricade would probably only have to survive as an integrated structure for a few tens of milliseconds. A recent series of controlled experiments that involved the detonation of one and two M107 rounds near rectangular water tanks with varying thicknesses of water was conducted by Boyle[19] and other colleagues at ARL. These experiments contained a strongly synergistic fragment and blast environment. While the results are still being evaluated, the preliminary analysis[19] indicates that high-speed (greater than 300 m/s) fragments along with possibly significant amounts of water moving at similar velocities have been recorded on the far side of a 3-foot-thick water tank. Destructive impacts were recorded on witness plates.

Two additional series of computations have recently been completed by the author. One is for a 1.17-m-thick rectangular water barricade and the other is for a 1.70-m-thick water barricade, each having the same height as the trapezoidal water barricade evaluated here. The same munitions stacks are modeled in the same way. Three standoffs, 3.05 m, 2.50 m, and 2.00 m are included to tie those computations to the ones reported herein. The effects of barricade shape (rectangular versus trapezoidal) and thickness (1.17 m versus 1.70 m) are significant. These studies will be reported promptly in separate publications. Additional computational studies of sand-filled barricades are in progress, as are studies of the impact of water and sand on simulated munitions.

INTENTIONALLY LEFT BLANK

REFERENCES

1. R.E. Lottero, "Responses of a Water Barricade and an Acceptor Stack to the Detonation of a Donor Munitions Stack," ARL-TR-1600, U.S. Army Research Laboratory, Aberdeen Proving Ground, MD, March 1998.

2. R.E. Lottero, "Numerical Modeling of the Responses of a Water Barricade and an Acceptor Stack to the Detonation of a Donor Munitions Stack," Proceedings of the 28th DDESB Explosives Safety Seminar, Orlando, FL, 18-20 August 1998.

3. R.L. Bell, M.R. Baer, R.M. Brannon, M.G. Elrick, A.V. Farnsworth, E.S. Hertel, S.V. Petney, S.A. Silling, and P.A. Taylor, "CTHGEN User's Manual and Input Instructions, Version 3.00," CTH Development Project, Sandia National Laboratories, Albuquerque, NM, 18 July 1996.

4. R.L. Bell, M.R. Baer, R.M. Brannon, M.G. Elrick, A.V. Farnsworth, E.S. Hertel, S.V. Petney, S.A. Silling, and P.A. Taylor, "CTH User's Manual and Input Instructions, Version 3.00," CTH Development Project, Sandia National Laboratories, Albuquerque, NM, 18 July 1996.

5. J.M. McGlaun, S.L. Thompson, L.N. Kmetck, and M.G. Elrick, "A Brief Description of the Three-Dimensional Shock Wave Physics Code CTH," SAND 89-0607, Sandia National Laboratories, Albuquerque, NM, July 1990.

6. R.L. Bell, M.R. Baer, R.M. Brannon, M.G. Elrick, E.S. Hertel Jr., S.A. Silling, and P.A. Taylor, "CTHGEN User's Manual and Input Instructions, Version 4.00," CTH Development Project, Sandia National Laboratories, Albuquerque, NM, 10 March 1998.

7. R.L. Bell, M.R. Baer, R.M. Brannon, M.G. Elrick, E.S. Hertel Jr., S.A. Silling, and P.A. Taylor, "CTH User's Manual and Input Instructions, Version 4.00," CTH Development Project, Sandia National Laboratories, Albuquerque, NM, 13 March 1998.

8. J. Starkenberg, K.J. Benjamin, and R.B. Frey, "Predicting Fragmentation Propagation Probabilities for Ammunition Stacks," ARL-TR-949, U.S. Army Research Laboratory, Aberdeen Proving Ground, MD, January 1996.

9. Headquarters, Department of the Army, "Technical Manual. Army Ammunition Data Sheets. Artillery Ammunition. Guns, Howitzers, Mortars, Recoilless Rifles, Grenade Launchers, and Artillery Fuzes." TM-43-0001-28, April 1977.

10. Department of the Army, "Ammunition and Explosives Safety Standards," AR 385-64, 22 May 1987.

11. G.I. Kerley and T.L.C. Frear, "Composition B-3 Detonation Products," SAND93-2131, Sandia National Laboratories, Albuquerque, NM, 1993.

12. G.I. Kerley, "CTH Reference Manual: The Equation of State Package," SAND91-0344, Sandia National Laboratories, Albuquerque, NM, 24 May 1991.

13. B.M. Dobratz and P.C. Crawford, "LLNL Explosives Handbook, Properties of Chemical Explosives and Explosive Simulants," UCRL-52997, Change 2, Lawrence Livermore National Laboratory, Livermore, CA, 31 January 1985.

14. Federal-Fabrics-Fibers, Inc., "Rapid Ammunition Barricade Technology Development," Small Business Innovative Research Contract DAAE30-97-C-1023, 10 March 1997.

15. F.H. Ree, "Equation of State for Water," UCRL-52190, Lawrence Livermore National Laboratory, Livermore, CA, December 1976.

16. G.I. Kerley, "Multiphase Equation of State for Iron," SAND93-0227, Sandia National Laboratories, Albuquerque, NM, 1993.

17. H.C. Graboske, Data for dry air, UCID-16901, December 1981 (modified March 1992).

18. T.P. Liddiard and J.W. Forbes, "A Summary Report of the Modified Gap Test and the Underwater Sensitivity Test," NSWC TR 86-350, Naval Surface Warfare Center, Silver Spring, MD, 12 March 1987.

19. V. Boyle, Private communication, U.S. Army Research Laboratory, Aberdeen Proving Ground, MD, 1998.

NO. OF COPIES ORGANIZATION

2 DEFENSE TECHNICAL INFORMATION CENTER
DTIC DDA
8725 JOHN J KINGMAN RD
STE 0944
FT BELVOIR VA 22060-6218

1 HQDA
DAMO FDQ
D SCHMIDT
400 ARMY PENTAGON
WASHINGTON DC 20310-0460

1 OSD
OUSD(A&T)/ODDDR&E(R)
R J TREW
THE PENTAGON
WASHINGTON DC 20301-7100

1 DPTY CG FOR RDE HQ
US ARMY MATERIEL CMD
AMCRD
MG CALDWELL
5001 EISENHOWER AVE
ALEXANDRIA VA 22333-0001

1 INST FOR ADVNCD TCHNLGY
THE UNIV OF TEXAS AT AUSTIN
PO BOX 202797
AUSTIN TX 78720-2797

1 DARPA
B KASPAR
3701 N FAIRFAX DR
ARLINGTON VA 22203-1714

1 NAVAL SURFACE WARFARE CTR
CODE B07 J PENNELLA
17320 DAHLGREN RD
BLDG 1470 RM 1101
DAHLGREN VA 22448-5100

1 US MILITARY ACADEMY
MATH SCI CTR OF EXCELLENCE
DEPT OF MATHEMATICAL SCI
MAJ M D PHILLIPS
THAYER HALL
WEST POINT NY 10996-1786

NO. OF COPIES ORGANIZATION

1 DIRECTOR
US ARMY RESEARCH LAB
AMSRL D
R W WHALIN
2800 POWDER MILL RD
ADELPHI MD 20783-1145

1 DIRECTOR
US ARMY RESEARCH LAB
AMSRL DD
J J ROCCHIO
2800 POWDER MILL RD
ADELPHI MD 20783-1145

1 DIRECTOR
US ARMY RESEARCH LAB
AMSRL CS AS (RECORDS MGMT)
2800 POWDER MILL RD
ADELPHI MD 20783-1145

3 DIRECTOR
US ARMY RESEARCH LAB
AMSRL CI LL
2800 POWDER MILL RD
ADELPHI MD 20783-1145

ABERDEEN PROVING GROUND

4 DIR USARL
AMSRL CI LP (305)

NO. OF COPIES	ORGANIZATION
1	DIRECTOR DEFENSE RSCH AND ENGNRNG DD TWP WASHINGTON DC 20301
1	COMMANDER FIELD COMMAND DSWA FCTTS E MARTINEZ KIRTLAND AFB NM 87115
1	DIRECTOR ADV RSCH PROJECTS AGNCY TECH LIB 3701 N FAIRFAX DR ARLINGTON VA 22203-1714
1	COMMANDER USA ARDEC AMSTA FSM W BARBER BLDG 94 PICATINNY ARSENAL NJ 07806-5000
1	COMMANDER USA ENGINEER DIVISION HNDED FD PO BOX 1500 HUNTSVILLE AL 35807
1	COMMANDER USA CORPS OF ENGNRS FT WORTH DSTRCT CESWF PM J PO BOX 17300 FT WORTH TX 76102-0300
1	COMMANDER USA RSCH OFFICE SLCRO D PO BOX 12211 RESEARCH TRIANGLE PARK NC 27709-2211
1	COMMANDER DAVID TAYLOR RSCH CTR TECH INFO CTR CODE 522 BETHESDA MD 20084-5000

NO. OF COPIES	ORGANIZATION
1	OFFICER IN CHARGE CIVIL ENGNRNG LAB NAVAL CONST BATTALION CTR TECH LIB CODE L31 PORT HUENEME CA 93041
1	COMMANDER NAVAL WEAPONS CTR TECH LIB CODE 533 CHINA LAKE CA 93555-6001
1	COMMANDER NSWC DAHLGREN DIVISION LIB CODE E23 DAHLGREN VA 22448-5000
1	COMMANDER NAVAL RSCH LAB TECH LIB CODE 2027 WASHINGTON DC 20375
1	COMMANDER NAVAL WEAPOONS EVAL FAC DOCUMENT CONTROL KIRTLAND AFB NM 87117
2	AIR FORCE ARMAMENT LAB AFATL DOIL AFATL DLYV EGLIN AFB FL 32542-5000
1	DIRECTOR LAWRENENC LIVERMORE NATL LAB TECH INFO DEPT L 3 PO BOX 808 LIVERMORE CA 94550
1	NAIC DXLA TECH LIB 4180 WATSON WAY WRIGHT PATTERSON AFB OH 45433-5648
1	KAMAN SCIENCES CORPORATION LIBRARY PO BOX 7463 COLORADO SPRINGS CO 80933-7463

NO. OF COPIES	ORGANIZATION
1	DIRECTOR SANDIA NATL LAB DOC CONTROL 3141 PO BOX 5800 ALBUQUERQUE NM 87185-5800
2	LOS ALAMOS NATL LAB RPT COLCTN CIC 14 MS P364 CID 14 MS P364 PO BOX 1663 LOS ALAMOS NM 87545
1	REPORT COLLECTION AGENCY RSCH LAB MS P362 PO BOX 7113 LOS ALAMOS NM 87544-7113
1	DIRECTOR SANDIA NATL LAB LIVERMORE LAB DOC CONTROL FOR THE LIB PO BOX 969 LIVERMORE CA 94550
1	DIRECTOR NASA LANGLEY RSCH CTR TECH LIB HAMPTON VA 23665
1	SUNBURST RECOVERY INC C YOUNG PO BOX 2129 STEAMBOAT SPRINGS CO 80477
2	SRI INTERNATIONAL J GRAN B HOLMES 333 RAVEWOOD AVE MENLO PARK CA 94025
2	DENVER RSCH INSTITUTE J WISOTSKI TECH LIB PO BOX 10758 DENVER CO 80210

NO. OF COPIES	ORGANIZATION
3	SOUTHWEST RSCH INSTITUTE C ANDERSON S MULLIN A B WENZEL PO DRAWER 28255 SAN ANTONIO TX 78228-0255
1	UNIVERSITY OF TEXAS ARL ELCTROMAG GROUP A TUCKER CAMPUS MAIL CODE F0250 AUSTIN TX 78712
1	UNIV OF MARYLAND R DICK RM 2168 ENGRG CLASSROOM BLDG COLLEGE PARK MD 20742-5121
1	US NAVAL ACADEMY TECH LIB 572 HOLLOWAY RD ANNAPOLIS MD 21402-5002
1	OLIN ORDNANCE RECH LIB J KIBIGER PRODUCT MATERIAL CONTROL 10101 9TH ST N ST PETERSBURG FL 33716
1	COMMANDER INDIAN HEAD DIV NSWC CODE 950T M SWISDAK 101 STRAUSS AVE INDIAN HEAD MD 20640-5035
1	COMMANDING OFFICER NFESC J TANCRETO ESC62 1100 23RD AVE BLDG 1100 PORT HUENEME CA 93043-4370
1	CHAIRMAN DOD EXPOSIVES SAFETY BOARD J WARD HOFFMAN BLDG 1 ROOM 856C 2461 EISENHOWER AVE ALEXANDRIA VA 22331-0600

NO. OF COPIES	ORGANIZATION
1	DEFENSE AMMOLOG ACTIVITY AMSTA AR AL D SCARBOROUGH PICATINNY ARSENAL NJ 07806-5000
1	US ARMY SOLDIER SYSTEMS CMD SSCNS WSO D LEMOINE KANSAS ST NATICK MA 01760-5018
5	USAE WATERWAYS EXP STN CEWES SD R P KINNEBREW B CARNES CEWES TL TECH LIB CEWES SD K DAVIS CEWES SS J WEATHERSBY 3909 HALLS FERRY RD VICKSBURG MS 39180-6199
1	DIR SNL ES HERTEL JR MS 0819 PO BOX 5800 ALBUQUERQUE NM 87185-0307
1	KERLEY PUB SUC G I KERLEY PO BOX 13835 ALBUQUERQUE NM 87192-3835

NO. OF COPIES	ORGANIZATION
	ABERDEEN PROVING GROUND
1	COMMANDER US ARMY TECOM AMSTE TE F L TELETSKI
	ABERDEEN PROVING GROUND (CONT)
1	COMMANDER USATC STEC LI
30	DIRECTOR USARL AMSRL WM MA W CHIN T MULKERN C PERGANTIS AMSRL WM PB B GUIDOS H EDGE P PLOSTINS P WEINACHT AMSRL WM T A M DIETRICH AMSRL WM TB V BOYLE P BAKER T DORSEY R FREY W HILLSTROM W LAWRENCE R LOTTERO (5CPS) E MCDOUGAL J STARKENBERG J WATSON AMSRL WM TC K KIMSEY D SCHEFFLER S SCHRAML AMSRL WM TD P KINGMAN M RAFTENBERG S SCHOENFELD P SIMMERS

REPORT DOCUMENTATION PAGE

Form Approved
OMB No. 0704-0188

1. AGENCY USE ONLY *(Leave blank)*	2. REPORT DATE	3. REPORT TYPE AND DATES COVERED
	May 1999	Final, 1 Jan 98 - 1 Dec 98

4. TITLE AND SUBTITLE
Standoff Variation Study I: Detonation of a Donor Munitions Stack and Responses of a Trapezoidal Water Barricade and an Acceptor Stack

5. FUNDING NUMBERS
JONO: 9810F1

6. AUTHOR(S)
Richard E. Lottero

7. PERFORMING ORGANIZATION NAME(S) AND ADDRESS(ES)
U.S. Army Research Laboratory
ATTN: AMSRL-WM-TB
Aberdeen Proving Ground, MD 21005-5066

8. PERFORMING ORGANIZATION REPORT NUMBER
ARL-TR-1943

9. SPONSORING/MONITORING AGENCY NAMES(S) AND ADDRESS(ES)
D. Scarborough
U.S. Army Defense Ammunition Logistics (Ammolog) Activity
Picatinny Arsenal, NJ 7806-5000

10.SPONSORING/MONITORING AGENCY REPORT NUMBER

11. SUPPLEMENTARY NOTES

12a. DISTRIBUTION/AVAILABILITY STATEMENT
Approved for public release; distribution is unlimited.

12b. DISTRIBUTION CODE

13. ABSTRACT *(Maximum 200 words)*

This report documents the fully coupled numerical modeling of the detonation of a simplified munitions stack in a temporary storage area and the subsequent effects on the immediate surroundings of the stack. Five plausible configurations of this munitions stack, referred to as the "donor" stack, an intervening water barricade, and an "acceptor" munitions stack are modeled in two-dimensional (2-D) Cartesian hydrocode computations using the CTH hydrodynamics computer code. The distance between each munitions stack and the barricade, referred to here as the "standoff" distance, is varied from one computation to the next, with the physical characteristics of the munitions stacks and barricade themselves remaining unchanged. The donor stack is modeled as an uncased, condensed, high-explosive charge with a rectangular cross section. The water barricade has a trapezoidal cross section, and the acceptor stack is a solid iron rectangle. The loadings on both the barricade and the acceptor stack are computed, as are their fully coupled responses to those loadings. Only a relatively weak inverse functional relationship with standoff distance was found in the barricade response. A moderate correlation with standoff distance, and a stronger correlation with the distance between the donor stack right face and the acceptor stack left face, were found for the acceptor stack response. The results are also compared with those of an earlier study on two uncoupled blast loading and response computations for one of the configurations.

14. SUBJECT TERMS	15. NUMBER OF PAGES
munitions survivability, detonation modeling, barricade, blast loading, hydrocode	69
	16. PRICE CODE

17. SECURITY CLASSIFICATION OF REPORT	18. SECURITY CLASSIFICATION OF THIS PAGE	19. SECURITY CLASSIFICATION OF ABSTRACT	20. LIMITATION OF ABSTRACT
UNCLASSIFIED	UNCLASSIFIED	UNCLASSIFIED	UL

INTENTIONALLY LEFT BLANK.

USER EVALUATION SHEET/CHANGE OF ADDRESS

This Laboratory undertakes a continuing effort to improve the quality of the reports it publishes. Your comments/answers to the items/questions below will aid us in our efforts.

1. ARL Report Number/Author ARL-TR-1943 (Lottero) Date of Report May 1999

2. Date Report Received _____

3. Does this report satisfy a need? (Comment on purpose, related project, or other area of interest for which the report will be used.) _____

4. Specifically, how is the report being used? (Information source, design data, procedure, source of ideas, etc.) _____

5. Has the information in this report led to any quantitative savings as far as man-hours or dollars saved, operating costs avoided, or efficiencies achieved, etc? If so, please elaborate. _____

6. General Comments. What do you think should be changed to improve future reports? (Indicate changes to organization, technical content, format, etc.) _____

CURRENT ADDRESS

_____
Organization

_____
Name E-mail Name

_____
Street or P.O. Box No.

_____
City, State, Zip Code

7. If indicating a Change of Address or Address Correction, please provide the Current or Correct address above and the Old or Incorrect address below.

OLD ADDRESS

_____
Organization

_____
Name

_____
Street or P.O. Box No.

_____
City, State, Zip Code

(Remove this sheet, fold as indicated, tape closed, and mail.)
(DO NOT STAPLE)